Lactobacillus rhamnosus GG attenuates tenofovir disoproxil fumarate-induced bone loss in male mice *via* gut-microbiota-dependent anti-inflammation

Hao Liu, Ranli Gu, Wei Li, Wen Zhou, Zhe Cong, Jing Xue, Yunsong Liu, Qiang Wei and Yongsheng Zhou

Ther Adv Chronic Dis

2019, Vol. 10: 1–23

DOI: 10.1177/2040622319860653

Abstract

Background: Although antiretroviral agents trigger bone loss in human immunodeficiency virus patients, tenofovir disoproxil fumarate (TDF) induces more severe bone damage, such as osteoporosis. While the mechanisms are unclear, probiotic supplements may be effective against osteoporosis.

Methods: C57BL6/J mice were administered with *Lactobacillus rhamnosus* GG (LGG)+TDF, TDF, and zoledronic acid+TDF, respectively. Bone morphometry and biomechanics were evaluated using microcomputed tomography, bone slicing, and flexural tests. The lymphocyte, proinflammatory cytokines, and intestinal permeability levels were detected using enzyme-linked immunosorbent assays, quantitative real-time polymerase chain reaction, and flow cytometry. The gut microbiota composition and metabolomics were analyzed using 16S recombinant deoxyribonucleic acid pyrosequencing and ultra-performance liquid-chromatography–quadrupole time-of-flight mass spectrometry.

Results: LGG administered orally induced marked increases in trabecular bone microarchitecture, cortical bone volume, and biomechanical properties in the LGG+TDF group compared with that in the TDF-only group. Moreover, LGG treatment increased intestinal barrier integrity, expanded regulatory T cells, decreased Th17 cells, and downregulated osteoclastogenesis-related cytokines in the bone marrow, spleen, and gut. Furthermore, LGG reconstructed the gut microbiota and changed the metabolite composition, especially lysophosphatidylcholine levels. However, the amount of N-acetyl-leukotriene E4 was the highest in the TDF-only group.

Conclusion: LGG reconstructed the community structure of the gut microbiota, promoted the expression of lysophosphatidylcholines, and improved intestinal integrity to suppress the TDF-induced inflammatory response, which resulted in attenuation of TDF-induced bone loss in mice. LGG probiotics may be a safe and effective strategy to prevent and treat TDF-induced osteoporosis.

Keywords: inflammatory response, *Lactobacillus rhamnosus* GG, microbial metabolomics, osteoporosis, tenofovir disoproxil fumarate

Received: 7 April 2019; revised manuscript accepted: 3 June 2019.

Correspondence to:
Yongsheng Zhou and Yunsong Liu
Department of Prosthodontics, Peking University School and Hospital of Stomatology and National Clinical Research Center for Oral Diseases and National Engineering Laboratory for Digital and Material Technology of Stomatology and Beijing Key Laboratory of Digital Stomatology, 22 Zhongguancun South Avenue, Haidian District, Beijing 100081, People's Republic of China
kqzhouysh@hsc.pku.edu.cn;
kqliuyunsong@sohu.com;

Qiang Wei
Key Laboratory of Human Disease Comparative Medicine, Chinese Ministry of Health, Beijing Key Laboratory for Animal Models of Emerging and Remerging Infectious Diseases, Institute of Laboratory Animal Science, Chinese Academy of Medical Sciences and Comparative Medicine Center, Peking Union Medical College, No.5, Panjiayuan, Nanli, Chaoyang District, Beijing 100021, People's Republic of China
weiqiang0430@cnilas.org

Hao Liu
Wen Zhou
The Central Laboratory, Peking University School and Hospital of Stomatology and National Clinical Research Center for Oral Diseases and National Engineering Laboratory for Digital and Material Technology of Stomatology and Beijing Key Laboratory of Digital Stomatology, Beijing, China

Ranli Gu
Department of Prosthodontics, Peking University School and Hospital of Stomatology and National Clinical Research Center for

Introduction

Since it was first approved in 2001, tenofovir disoproxil fumarate (TDF) has been widely used in first-line treatment of human immunodeficiency virus (HIV) and hepatitis B virus (HBV) infections worldwide. As part of the highly active

Oral Diseases and National Engineering Laboratory for Digital and Material Technology of Stomatology and Beijing Key Laboratory of Digital Stomatology, Beijing, China

Wei Li
Department of Oral Pathology, Peking University School and Hospital of Stomatology and National Clinical Research Center for Oral Diseases and National Engineering Laboratory for Digital and Material Technology of Stomatology and Beijing Key Laboratory of Digital Stomatology, Beijing, China

Zhe Cong
Jing Xue
Key Laboratory of Human Disease Comparative Medicine, Chinese Ministry of Health, Beijing Key Laboratory for Animal Models of Emerging and Remerging Infectious Diseases, Institute of Laboratory Animal Science, Chinese Academy of Medical Sciences and Comparative Medicine Center, Peking Union Medical College, Beijing 100021, China

antiretroviral therapy (HAART), TDF plays an antiretroviral role by inhibiting adenine analog reverse transcription and dramatically improves the survival of patients with HIV or HBV.[1] However, there are increasing concerns about TDF-induced osteopenia and osteoporosis as life expectancy is prolonged among patients with HIV or HBV.[2] Many studies have shown that HAART aggravates bone loss in HIV or HBV patients because of T-cell reconstitution.[3,4] However, the magnitude of bone resorption triggered by TDF is larger compared with other anti-HIV agents.[5,6] Hence, the mechanisms of TDF-induced bone loss may be more complicated than previously believed.

Osteoporosis is a chronic syndrome of excessive skeletal fragility, which is characterized by bone mass loss and bone microarchitecture deterioration. However, there are at least two kinds of specific precipitating factors for osteoporosis in patients infected by retrovirus. First, in patients with HIV for example, viral infection should be taken into account for osteoporosis.[7] Second, antiretroviral therapy (ART), especially nucleotide reverse-transcriptase inhibitors (NRTIs) like TDF, also play a key part in bone loss.[8] Thus, osteoporosis has the characteristics of high risk and young age for the retrovirus-infected population.[9] Epidemiological studies revealed there was a two- to fivefold-higher fracture incidence in HIV-infected subjects than in uninfected subjects.[10] However, HIV infection is a chronic fatal syndrome that cannot be completely eliminated from a mammalian host. Hence, there is an urgent need to alleviate TDF-induced osteoporosis in retrovirus-infected populations that are chronically administered with TDF.

Currently, there are two major pharmacological approaches to protect against osteoporosis: anabolic agents to stimulate bone formation, such as parathyroid hormone; and antiresorptive agents to inhibit bone resorption, such as bisphosphonates, calcitonin, raloxifene, and estrogen. Indeed, these medications improve bone mineral density (BMD) and reduce the risk of fractures in the initial years; however, their long-term safety and efficacy are the subject of ongoing concern.[11] Therefore, the accumulation of various negative factors for osteoporosis have increased the suffering of the retrovirus-infected population. Accordingly, safe and effective new treatments against TDF-induced osteoporosis should be explored.

The human gut is colonized by trillions of metazoans and comprises a diverse microecosystem known as the gut microbiota.[12] Importantly, several recent lines of evidence supported the hypothesis that the gut microbiota has an effect on bone homeostasis.[13] *Lactobacillus rhamnosus* GG (LGG), a type of probiotic from the gut of healthy individuals, is characterized by high and sustained adhesiveness to the intestinal mucosa.[14] LGG ameliorates alcohol-induced liver injury by improving intestinal integrity.[15] Moreover, administration of LGG improved the prognosis of pneumonia induced by *Pseudomonas aeruginosa* by upregulating regulatory T cell (Treg) levels and downregulating the systemic inflammatory response.[16] Therefore, we hypothesized that LGG could increase intestinal barrier integrity and downregulate the systemic inflammatory response, resulting in attenuation of TDF-induced bone loss. In addition, considering the efficacy and safety of TDF, clinical research has shown that the HIV ribonucleic acid (RNA) viral load remained stable in the blood of HIV-infected patients and no adverse events were reported when LGG was administered orally, indicating that LGG was well tolerated by patients with HIV.[17] In the present study, we aimed to evaluate the effects of LGG oral administration on TDF-induced bone loss in mice, and to further explore the underlying mechanism of these effects *in vitro* and *in vivo*.

Materials and methods

Bacterial strain, reagents, and antibodies

LGG (accession number 53103) and *Escherichia coli* (accession number 25922) were purchased from ATCC (Rockville, MD, USA). De Man, Rogosa, and Sharpe (MRS) broth and Luria-Bertani (LB) broth were purchased from OXOID (Hampshire, UK). TDF, zoledronic acid (ZOL), FD4 (fluorescein-isothiocyanate–dextran), calcein, alizarin-3-methyliminodiacetic acid, phorbol 12-myristate 13-acetate (PMA), and ionomycin were purchased from Sigma–Aldrich (Saint Louis, MO, USA). GolgiStop was obtained from BioLegend (San Diego, CA, USA). Fluorescein-isothiocyanate-labeled antimouse CD4 (cat#11-0041-81), allophycocyanin (APC)-labeled antimouse CD25 (cat#17-0251-81), phycoerythrin (PE)-labeled antimouse forkhead box P3 (FOXP3; cat#12-5773-82), and Peridinin chlorophyll protein complex (PerCP)/Cy5.5-labeled anti-mouse

interleukin (IL)-17A (cat#45-7177-82) were purchased from eBioscience (San Diego, CA, USA). Roswell Park Memorial Institute (RPMI) 1640 medium, fetal bovine serum (FBS), 100 U/ml penicillin G, and 100 mg/ml streptomycin were obtained from Gibco (Grand Island, NY, USA).

Culture of LGG and E. coli

LGG and *E. coli* were cultured in MRS broth and LB broth at 37°C in accordance with the ATCC guidelines, respectively. In brief, the bacteria were harvested from broth by centrifugation. Colony forming units (CFUs) were counted by dilution and streaking on agar plates at 37°C overnight using Easy Spiral Pro (Interscience, St. Nom, France).

Animals and administration procedure

Mice aged 6 weeks and male (C57BL6/J) were purchased from Vital River Inc. (Beijing, China). The mice were housed under specific pathogen-free conditions at the Peking University School and Hospital of Stomatology. They were allowed free access to a sterilized maintenance diet and autoclaved water in a 12 h light–dark cycle at a room temperature of 21 ± 2°C. All animal experiments were approved by the Animal Care and Use Committee of Peking University Health Science Center (approval number: LA2016305; Beijing, China).

The mice were randomly assigned to five groups after acclimatization for 1 week: (a) Sham group: the mice were administered with normal saline (NS) vehicle by oral gavage; (b) LGG+TDF group: the mice were administered by oral gavage with 0.86 mg TDF [43 mg/kg body weight (BW), dissolved in NS] every day according to the body surface area between mice and humans (300 mg/d TDF for human),[18] and orally administered with 5×10^8 CFU LGG (10^9 CFU/ml, dissolved in NS) twice a week; (c) *E. coli*+TDF group: the mice were administered by oral gavage with the same dose of TDF solution as the LGG group every day and orally administered with 5×10^8 CFU *E. coli* dissolved in NS (10^9 CFU/ml) twice a week; (d) TDF group: the mice were administered by oral gavage with TDF solution in the same dose of the above groups every day (negative control); (e) ZOL+TDF group: as a positive control, the mice were injected with ZOL (100 μg/kg BW) subcutaneously once a week for the first 4 weeks and orally administered with TDF solution at the same dose as the above groups. The BW of mice was recorded weekly. The mice were sacrificed at 8 weeks after administration. Tibiae were dissected thoroughly free from soft tissue. The tips of the tibiae were removed and bone marrow (BM) was harvested by inserting a syringe needle into one end of the bone and flushing with RPMI 1640 medium, as previously described.[19] Thereafter, the cells were cultured in maintenance medium (RPMI 1640 medium containing 10% FBS, 100 U/ml penicillin G, and 100 mg/ml streptomycin) at 37°C in an incubator with an atmosphere comprising 95% air and 5% CO_2. After 48 hours, the cell supernatants were collected for enzyme-linked immunosorbent assay (ELISA) detection.

Intestinal permeability tests

To assess the intestinal barrier function mediated by paracellular permeability *in vivo*, intestinal permeability tests using fluorescently labeled dextran were performed.[20] In brief, FD4 (22 mg/ml) was administered at 11 mg per mouse in every group by oral gavage. At 4 hours after administration, the mouse serum was obtained through terminal cardiac puncture under general anesthesia. The serum FD4 concentration was calculated using a microtiter plate luminometer (Enspire Perkin Elmer, Waltham, MA, USA) using excitation at 485 nm and emission at 530 nm.

Microcomputed tomography (CT) analyses

To assess the bone mass and microarchitecture among the five groups, microcomputed tomography (micro-CT) was performed using the Inveon MM system (Siemens, Munich, Germany) as previously described.[21] In brief, the specimens were scanned at an effective pixel size of 8.89 μm, a voltage of 60 kV, a current of 220 μA, and an exposure time of 1500 ms in each of the 360 rotational steps, *in vivo* and *ex vivo*. The images consisted of 1536 slices and had a voxel size of 8.89 μm in all three axes. Three-dimensional (3D) visualization images were reconstructed by two-dimensional images and the parameters were calculated using Inveon Research Workplace (Siemens) as follows: BMD, bone mineral content (BMC), cortical bone area/total bone area (%Ct.Ar), bone volume/total volume (BV/TV),

trabecular number (Tb.N), bone surface area/bone volume (BS/BV), trabecular separation (Tb.Sp), and trabecular thickness (Tb.Th) in the region of interest of the femur (1–2 mm below the distal growth plate; Figure S1), L4 vertebra (trabecular bone of the centrum), mandible (septa interradicularia mandibulaeta and mandibular angle), and growth plates, as described previously[22–24] according to guidelines set by the American Society for Bone and Mineral Research.[25]

Dynamic histomorphometric analyses

To evaluate their dynamic histomorphometry, mice were injected with calcein [20 mg/kg BW, intraperitoneal (i.p.)] and alizarin-3-methyliminodiacetic acid (30 mg/kg BW, i.p.) at 10 and 3 days before euthanasia, respectively. After sacrifice, the tibia was fixed, dehydrated, and embedded in destabilized methyl methacrylate resin to make slices of undecalcified bones. Next, the sections were ground and polished to 40–60 μm using an EXAKT precision cutting and grinding system (EXAKT Apparatebau, Hamburg, Germany) and stained with toluidine blue. The mineral apposition rate (MAR) and bone formation rate/bone surface (BFR/BS) were detected using the Bioquant software (BioQuant, San Diego, CA, USA).[26]

Hematoxylin and eosin (H&E) staining and tartrate-resistant acidic phosphatase (TRAP) staining

To further explore the histomorphology of the femur and gut, tissue slicing, and H&E staining were performed. First, the femur was decalcified for 2 weeks in 10% EDTA (pH 7.4). Thereafter, the specimens were dehydrated, followed by embedding in paraffin. Sections about of 5 mm thick were made and stained with H&E.[19] In addition, tartrate-resistant acidic phosphatase (TRAP) staining was performed using a TRAP staining kit (Sigma–Aldrich).

Biomechanical assays

To investigate the biomechanics of the femur, 3-point flexural tests were performed. The femurs were subjected to push down by a plunger at a speed of 1.0 mm/min using a servohydraulic testing device (Instron 4302, Norwood, MA, USA), as previously described.[27] Load-deformation curves were recorded during the bending process. The analysis area was the mid-diaphysis of the femur. The parameters were calculated as follows: The maximum load, energy to ultimate load, Young's modulus, stiffness, and breaking energy.

Assay for biochemical markers

To evaluate the serum biochemical markers of bone turnover and proinflammatory cytokines, the associated ELISAs were performed according to the manufacturer's instructions.[21] Specifically, ELISA for procollagen 1 N-terminal peptide (P1NP), receptor activator of nuclear factor kappa-B ligand (RANKL), and cross-linked carboxy-terminal telopeptide of type 1 collagen (CTX-1; IDS, Frankfurt, Germany) were detected for bone turnover; tumor necrosis factor alpha (TNF-α) and interleukin 17 (IL-17) were also measured using commercial ELISA kits (eBioscience, San Diego, CA, USA) to explore levels of inflammatory markers in the serum and cell supernatant. Moreover, the serum levels of calcium (Ca) and phosphorus (P) were measured using a plasma emission spectrometer (iCAP 6000; Thermo Fisher Scientific, Waltham, MA, USA). In addition, to assess whether LGG administration disturbed the TDF levels in blood, the serum TDF concentrations in the five groups were detected using an Agilent 1260 HPLC instrument (Agilent Technologies, Santa Clara, CA, USA) as previously described.[28] Samples were measured at least in duplicate.

Flow cytometry

To explore the effects on Treg and Th17 cells in this study, fluorescence-activated cell sorting (FACS) was used as previously described.[29] First, single-cell suspensions of the spleen, BM, and mesenteric lymph node (MLN) were prepared in RPMI 1640 culture medium. Next, the cells were incubated at 37°C for 4 h with PMA (50 ng/ml) and ionomycin (1 μg/ml) before adding GolgiStop (1 μg/ml). The cells were then stained with fluorescein-isothiocyanate-labeled anti-CD4 or APC-labeled anti-CD25 antibodies to detect surface markers, followed by intracellular staining with PerCp/Cy5.5 anti-IL-17A or PE anti-FOXP3 antibodies. Cells were detected using an LSRII flow cytometer (BD Biosciences,

San Jose, CA, USA). The results are shown as cell frequency (%).

RNA extraction and quantitative real-time PCR (qPCR)

RNA was extracted from femurs and 10-mm piece of intestine from mice using the Qiagen RNeasy Mini kit (Qiagen, Hilden, Germany) according to the manufacturer's instructions. First-strand complementary deoxyribonucleic acid (cDNA) was then synthesized using a reverse-transcription system (Takara, Kyoto, Japan). The relative abundance of the cDNA was assessed using quantitative polymerase chain reaction (qPCR) analysis using the 7500 Real-Time PCR Detection System (Applied Biosystems, Foster City, CA, USA). The following thermal settings were used: 95°C for 10 min, followed by 40 cycles of 95°C for 15 s and 60°C for 1 min. The primers used are listed in Table S1. The data were analyzed using the $2^{-\Delta CT}$ method with normalization to *Gapdh* expression.[30] Samples were measured at least in duplicate.

Gut microbiota composition analysis

To evaluate the bacterial diversity and community structure of the gut microbiota in the five groups, mice feces were analyzed *via* 16S recombinant deoxyribonucleic acid (rDNA) gene analysis, as previously described.[31] Briefly, feces were collected from the five groups of mice and total genomic DNA of the gut microbiota was extracted using a QIAamp DNA Mini Kit (Qiagen). Subsequently, the 16S rDNA V3–V4 region was amplified using universal primers for 16S V3–V4: 338F-806R. Next, the PCR products were purified, quantified, and sequenced using the MiSeq platform (Auwigene Co., Beijing, China) according to the vendor's standard protocols. The raw metagenomic data of the feces samples in the five groups have been deposited at the Sequence Read Archive of the National Center for Biotechnological Information under accession number SRP162310.

The pyrosequencing data were analyzed using the Quantitative Insights Into Microbial Ecology (QIIME) software package (QIIME development team, USA). Specifically, the raw sequences were identified as valid sequences for further analysis after low-quality sequences were excluded. High-quality sequences were clustered into operation taxonomic units (OTUs) at a similarity over 97% using Usearch (Edgar, USA).

To show the shared and unique OTUs among the groups, a Venn diagram was constructed according to quantity of OTUs in the group. However, for the alpha diversities, Tukey's test was used to compare the significant differences among the five groups. Moreover, beta diversity analysis was performed to assess the similarity of the gut microbiota community structures among the five groups according to UniFrac distances, using a weighted algorithm and visualized *via* principal coordinate analysis (PCoA). Furthermore, the taxa abundances at the phylum, class, order, family, genus, and species levels were statistically evaluated and graphed for the differences among the five groups. Thereafter, the linear discriminant analysis effect size (LEFSe) was calculated to show differentially relative abundances of the species based on a p value of 0.05 and a linear discriminant analysis (LDA) threshold of 3.0. The network analysis was visualized based on the genera (rho >0.6, $p<0.01$).

Metabolomics analysis of fecal sample using UPLC-Q-TOF/MS

To identify the differential metabolites between the LGG and TDF groups, metabolomics analysis of fecal sample between the two groups was performed using ultra-performance liquid-chromatography–quadrupole time-of-flight mass spectrometry (UPLC-Q-TOF/MS), as previously described.[32] First, fecal samples were prepared and the resulting supernatants were used for analysis together with an internal standard. Second, UPLC-Q-TOF/MS analysis was conducted using an ACQUITY UPLC I-Class system coupled with a VION IMS QTOF mass spectrometer (Waters Corporation, Milford, USA). To evaluate the data repeatability, the quality control and blank control samples were added into a set of samples. Thereafter, the raw data were analyzed to generate a data set using the progenesis QI software (Waters Corporation). Next, the data set was imported into the SIMCA software package (version 14.0, Umetrics, Umeå, Sweden) to carry out principal component analysis and orthogonal partial least-squares-discriminant analysis (OPLS-DA) between two groups. Variables with a variable importance in the projection (VIP)

>1.0 were deemed to contribute to group discrimination in the OPLS-DA model. The metabolites with a VIP >1.0 and $p<0.05$ in the data set were considered as markers responsible for the differentiation between the two groups by multivariate and univariate statistical methods. Lastly, the Kyoto Encyclopedia of Genes and Genomes (KEGG) database was used to link these metabolites to metabolic pathways to further interpret their biological significance.

Statistical analysis

The data are expressed as the mean ± standard deviation (SD). Statistical Package for Social Sciences v16.0 (IBM Corp., Armonk, NY, USA) was used to perform the statistical analyses. Independent two-tailed student's *t* test or one-way analysis of variance (ANOVA) with *post hoc* test application of least significant difference (LSD) for multiple comparisons were carried out. *p* values less than 0.05 were considered significant. Statistical analysis was performed using GraphPad Prism 5 (GraphPad Inc., La Jolla, CA, USA).

Results

Supplementation with LGG attenuates bone loss induced by TDF

First, the results of the differences of BW between baseline and 8 weeks showed that the LGG+TDF group had a dramatically lower BW than that of the *E. coli*+TDF and TDF groups at 8 weeks ($p<0.05$, respectively). However, the difference in BW for the TDF group was highest among the five groups ($p<0.05$, respectively; Figure S2). Next, to investigate the role of LGG in TDF-induced bone loss, BMD and bone morphometry of the femur were carried out to assess the mass and microarchitecture of bone using micro-CT, and the results are shown in Table 1 and Figure 1(a). At 8 weeks, the LGG+TDF group exhibited a substantial increase in the BM BMD (Ma.BMD), %Ct.Ar, BV/TV, Tb.N, and a significant decrease in the BS/BV and Tb.Sp compared with those in the *E. coli*+TDF and TDF groups ($p<0.05$, respectively), which was consistent with the Sham group. Notably, the ZOL+TDF group had the highest Ma.BMD, BMC in BM (Ma.BMC), BV/TV, and Tb.Th and the lowest BS/BV and Tb.Sp among the five groups ($p<0.05$, respectively). Besides, ZOL+TDF group had a significantly increased %Ct.Ar compared with the *E. coli*+TDF and TDF groups ($p<0.05$, respectively). Moreover, the LGG+TDF group had a markedly increased Tb.N compared with that in the ZOL+TDF group ($p<0.05$). Notably, the bone mass and morphometry of the centrum and mandible in the LGG+TDF group were similar to those of the femur (Table S2).

Surprisingly, bone regeneration-related parameters in the LGG+TDF group generally showed better effects at 4 weeks than at 8 weeks (Table S3 and Figure S3). In particular, the BV/TV and Ma.BMD in the LGG+TDF and Sham groups showed significant increases at 4 weeks compared with baseline, and dramatic decreases at 8 weeks compared with those at 4 weeks ($p<0.05$, respectively). However, there were continuous decreases for these two parameters in the *E. coli*+TDF and TDF groups at 4 and 8 weeks compared with baseline ($p<0.05$, respectively). Besides, the BV/TV and Ma.BMD values in the ZOL+TDF group showed a significant increase at 4 and 8 weeks compared with baseline [$p<0.05$, respectively; Figure 1(b,c)]. Moreover, the %Ct.Ar of the LGG+TDF, *E. coli*+TDF, TDF, and ZOL+TDF groups increased significantly at 4 or 8 weeks compared with baseline [$p<0.05$, respectively; Figure 1(d)].

To further assess bone regeneration, growth plate thickness was measured. The results revealed that the growth plates in the LGG+TDF group were the thickest among the five groups ($p<0.05$, respectively), as measured by micro-CT and histology. Moreover, there were more hypertrophic chondrocytes in the growth plate of the LGG+TDF group compared with those in the other groups, indicating that more active endochondral ossification occurred in the LGG group. Besides, the *E. coli*+TDF and TDF groups had significantly thinner growth plates compared with those of the ZOL+TDF and Sham groups [$p<0.05$, respectively; Figure 2(a,b)].

Consistent with abovementioned static indices of bone microarchitecture, dynamic histomorphometric analyses using double fluorescent labeling also showed that the MAR and BFR/BS ratio in the LGG+TDF group were the highest among the five groups ($p<0.05$, respectively). Moreover, the MAR of the ZOL+TDF group was the lowest

Table 1. BMD and bone histomorphometry for femur in the five groups at 8 weeks ($n = 10–12$).

Groups	Sham	LGG+TDF	*E. coli*+TDF	TDF	ZOL+TDF
Femur:					
Ma.BMD (mg/cm^3)	544.172 ± 46.588	565.929 ± 57.65	415.57 ± 18.319*,#	421.582 ± 14.481*,#	1231.783 ± 124.543*,#,%,$
Ma.BMC (mg)	0.739 ± 0.132	0.868 ± 0.169	0.551 ± 0.055	0.623 ± 0.056	2.387 ± 0.324*,#,%,$
%Ct.Ar	28.438 ± 2.084	27.872 ± 0.671	25.131 ± 0.346*,#	21.908 ± 2.028*,#,%	27.574 ± 1.564%,$
BV/TV (%)	25.407 ± 3.821	26.323 ± 3.947	16.757 ± 2.158*,#	16.223 ± 0.822*,#	94.028 ± 2.278*,#,%,$
BS/BV (mm^{-1})	44.029 ± 6.805	45.577 ± 2.641	55.382 ± 1.641*,#	51.062 ± 1.498*,#	10.941 ± 3.163*,#,%,$
Tb.Th (mm)	0.045 ± 0.01	0.044 ± 0.003	0.038 ± 0.003	0.039 ± 0.001	0.194 ± 0.017*,#,%,$
Tb.N (mm^{-1})	6.049 ± 0.343	6.008 ± 0.536	4.594 ± 0.469*,#	4.138 ± 0.111*,#	5.078 ± 0.565*#,$
Tb.Sp (mm)	0.129 ± 0.027	0.12 ± 0.025	0.192 ± 0.021*,#	0.203 ± 0.007*,#	0.011 ± 0.007*#,%,$
N.Oc/BS (mm^{-1})	5.43 ± 0.464	4.36 ± 0.606	10.82 ± 1.927*,#	12.33 ± 1.861*,#	4.64 ± 0.419%,$
Oc.S/BS (%)	22.11 ± 2.855	19.269 ± 1.376	36.067 ± 1.903*,#	37.746 ± 3.254*,#	16.568 ± 2.136%,$

Parameters on BMD and bone microarchitecture were measured in the distal femur using micro-CT. Data are expressed as mean ± SD. All data were normally distributed according to the Shapiro–Wilk normality test and analyzed using two-way ANOVA and *post hoc* tests applying the LSD correction for multiple comparisons.
*$p < 0.05$ compared with the Sham group.
#$p < 0.05$ compared with the LGG+TDF group.
%$p < 0.05$ compared with the *E. coli*+TDF group.
$$p < 0.05$ compared with TDF group.
ANOVA, analysis of variance; BMD, bone mineral density; CT, computed tomography; %Ct.Ar, cortical bone area/total bone area; BS/BV, bone surface area/bone volume; BV/TV, bone volume/total volume; LGG, *Lactobacillus rhamnosus* GG; LSD, least significant difference; Ma.BMC, bone mineral content in bone marrow; Ma.BMD, bone mineral density in bone marrow; N.Oc/BS, osteoclast number/bone surface; Oc.S/BS: osteoclast surface/bone surface; Tb.N, trabecular number; Tb.Sp, trabecular separation; Tb.Th, trabecular thickness; SD, standard deviation; TDF, tenofovir disoproxil fumarate; ZOL, zoledronic acid.

among the five groups ($p < 0.05$, respectively). Besides, the BFR/BS ratios of the *E. coli*+TDF, TDF, and ZOL+TDF groups were lower than that in the Sham group [$p < 0.05$, respectively; Figure 2(c,d)].

As expected, the serum P1NP level of the LGG+TDF group was the highest among the five groups ($p < 0.05$, respectively). Besides, the ZOL+TDF group had a dramatically increased P1NP level compared with the *E. coli*+TDF and TDF groups [$p < 0.05$, respectively; Figure 3(a)]. By contrast, the serum CTX-1 levels in the LGG+TDF and Sham groups were markedly decreased compared with those in the *E. coli*+TDF, TDF, and ZOL+TDF groups ($p < 0.05$, respectively) [Figure 3(b)]. Considering the antiviral efficacy of TDF, the serum TDF concentration was detected using HPLC. Interestingly, except for the Sham group (no TDF administered), only the ZOL+TDF group had a significantly decreased serum TDF concentration compared with that in the LGG+TDF and TDF groups [$p < 0.05$, respectively; Figure 3(c)].

Biomechanics is a key index for osseous evaluation. The results of the biomechanical parameters suggested that the maximum load, energy to ultimate load, Young's modulus, stiffness, and breaking energy in the LGG+TDF group were markedly increased compared with those in the *E. coli*+TDF or TDF groups ($p < 0.05$, respectively). Besides, the maximum load, energy to ultimate load, and stiffness of the ZOL+TDF group were significantly increased compared with those of the *E. coli*+TDF or TDF groups [$p < 0.05$, respectively; Figure 3(d)].

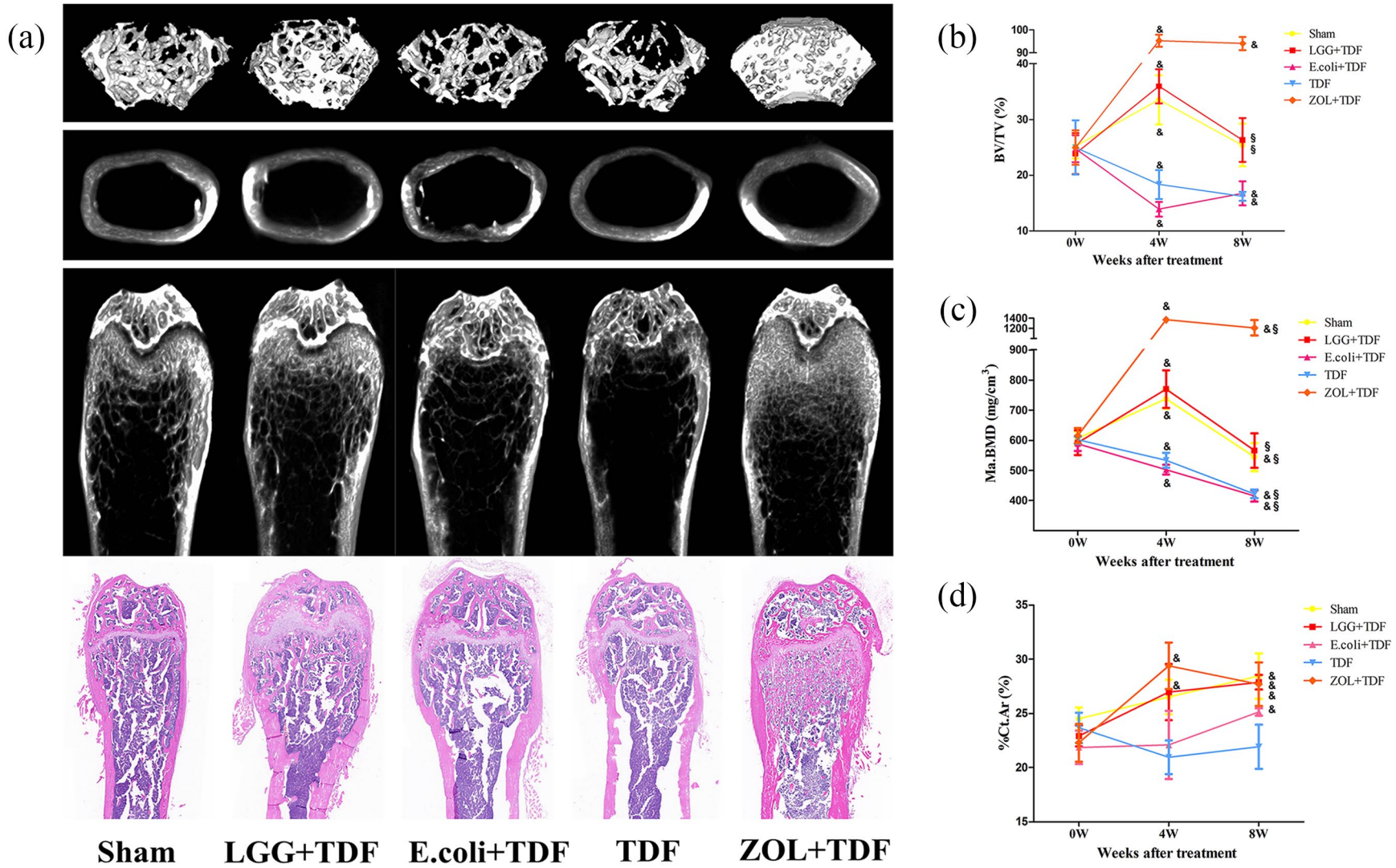

Figure 1. Supplementation with LGG attenuated TDF-induced bone microarchitecture destruction at 4 and 8 weeks.
(a) Representative images of the trabecular bone and cortical bone in the femur at 8 weeks. Parameters for BV/TV (b), Ma.BMD (c), and %Ct.Ar (d) of the femur at baseline, and 4 and 8 weeks. $n = 10–12$ mice per group in all panels. Data are expressed as mean ± SD. All data were normally distributed according to the Shapiro–Wilk normality test and analyzed using two-way ANOVA and *post hoc* tests applying the LSD correction for multiple comparisons.
$^{\&}p < 0.05$ compared with baseline.
$^{\S}p < 0.05$ compared with the 4-week (4W) time point.
ANOVA, analysis of variance; LGG, *Lactobacillus rhamnosus* GG; LSD, least significant difference; TDF, tenofovir disoproxil fumarate; BV/TV, bone volume/total volume; Ma.BMD, bone mineral density in bone marrow; %Ct.Ar, cortical bone area/total bone area; SD, standard deviation; ZOL, zoledronic acid.

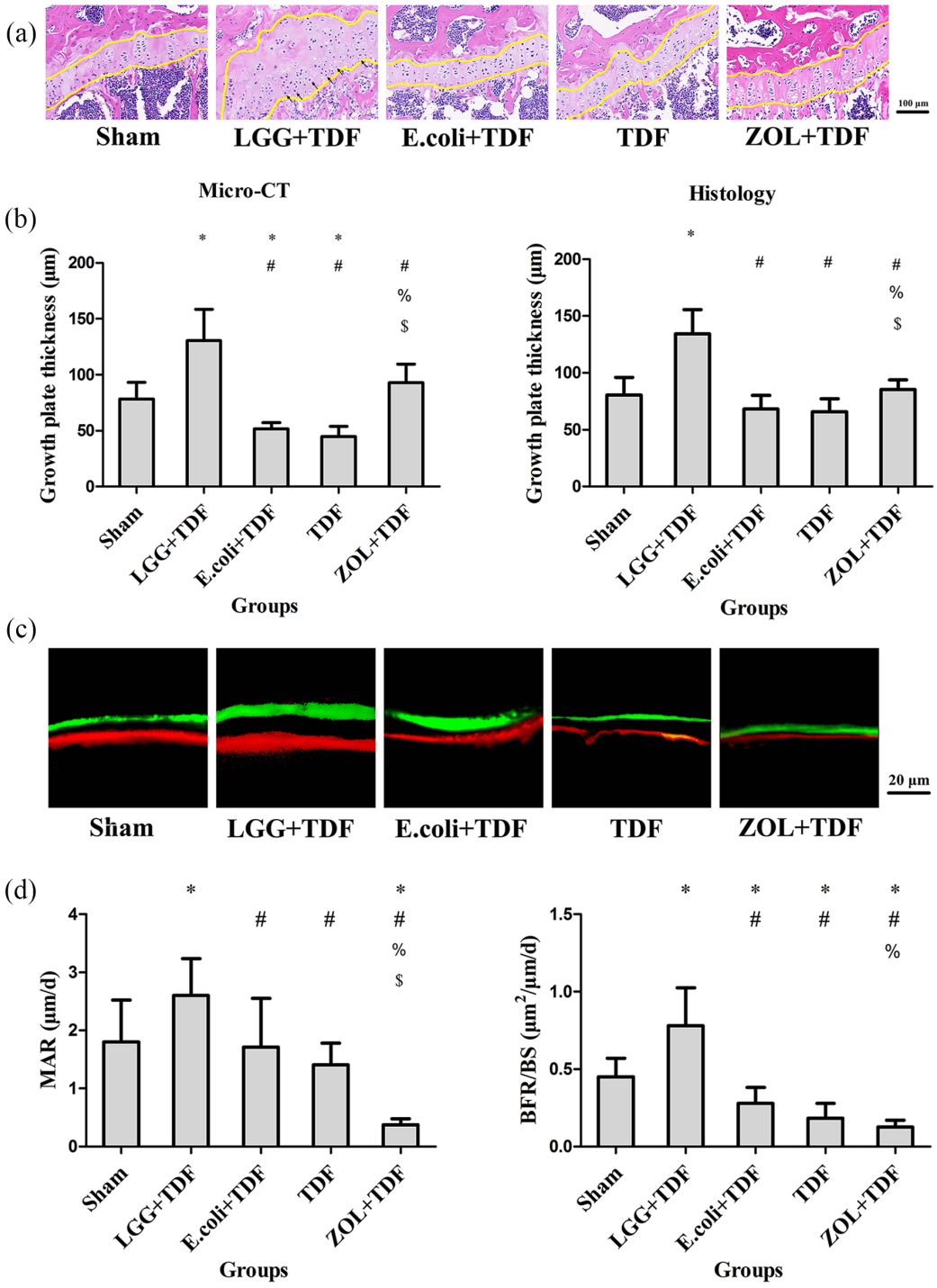

Figure 2. Administration of LGG promoted bone turnover and endochondral ossification at 8 weeks.
(a) Representative images of the growth plate in the femur (yellow lines indicate the growth plate; black arrows indicate hypertrophic chondrocytes). Scale bar = 100 μm. (b) Growth plate thickness measured in the femur. (c) Representative fluorescence images obtained from tibias after double labeling. Scale bar = 20 μm. (d) Dynamic MAR and BFR/BS measured from the tibia. $n = 10$ mice per group in all panels. Data are expressed as mean ± SD. All data were normally distributed according to the Shapiro–Wilk normality test and analyzed using two-way ANOVA and *post hoc* tests applying the LSD correction for multiple comparisons.
*$p < 0.05$ compared with the Sham group.
#$p < 0.05$ compared with the LGG+TDF group.
%$p < 0.05$ compared with *E. coli*+TDF group.
$$p < 0.05$ compared with the TDF group.
ANOVA, analysis of variance; BFR/BS, bone formation rate/bone surface; LGG, *Lactobacillus rhamnosus* GG; LSD, least significant difference; MAR, mineral apposition rate; SD, standard deviation; TDF, tenofovir disoproxil fumarate; ZOL, zoledronic acid.

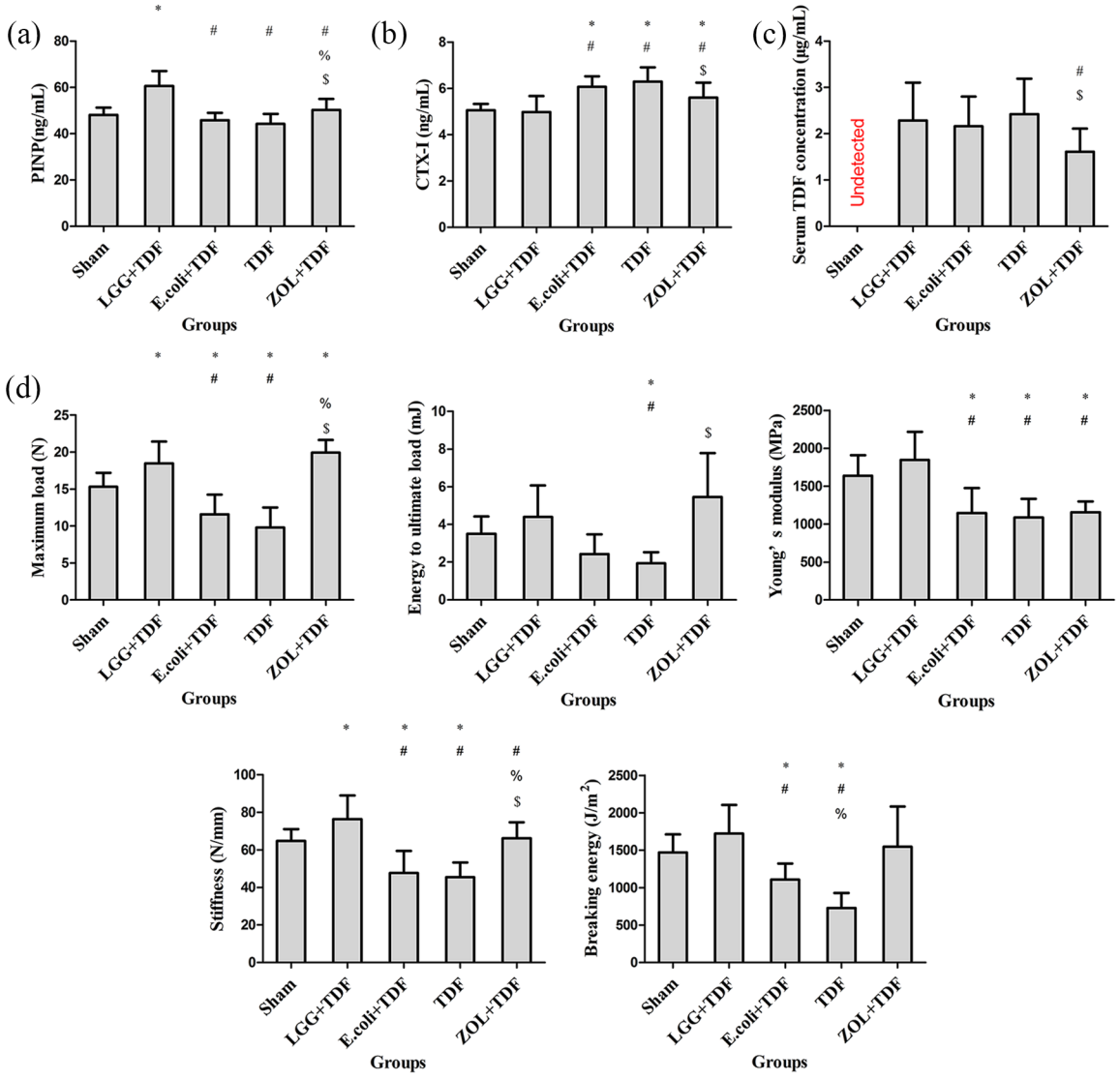

Figure 3. Administration of LGG improved serum bone turnover markers and biomechanical properties at 8 weeks. Serum levels of P1NP (marker of bone formation) (a), CTX-1 (marker of bone resorption) (b), and the TDF concentration (serum TDF concentration was undetectable because no TDF was administered in the Sham group) (c). (d) The biomechanical parameters of maximum load, energy to ultimate load, Young's modulus, stiffness, and breaking energy were evaluated using a 3-point flexural test. $n = 8$–10 mice per group in all panels. Data are expressed as mean ± SD. All data were normally distributed according to the Shapiro–Wilk normality test and analyzed using two-way ANOVA and *post hoc* tests applying the LSD correction for multiple comparisons.
*$p < 0.05$ compared with the Sham group.
#$p < 0.05$ compared with the LGG+TDF group.
%$p < 0.05$ compared with the *E. coli*+TDF group.
$$p < 0.05$ compared with the TDF group.
ANOVA, analysis of variance; CTX-1, cross-linked carboxy-terminal telopeptide of type 1 collagen; LGG, *Lactobacillus rhamnosus* GG; LSD, least significant difference; P1NP, procollagen 1 N-terminal peptide; SD, standard deviation; TDF, tenofovir disoproxil fumarate; ZOL, zoledronic acid.

LGG administration protects against osteoclastogenesis and associated inflammatory responses in BM

To determine whether bone loss was associated with osteoclastogenesis, the results indicated that the N.Oc/BS and Oc.S/BS of LGG+TDF, Sham, and ZOL+TDF groups significantly decreased compared with the *E. coli*+TDF and TDF groups ($p < 0.05$, respectively), which were similar with the images on TRAP staining [Table 1

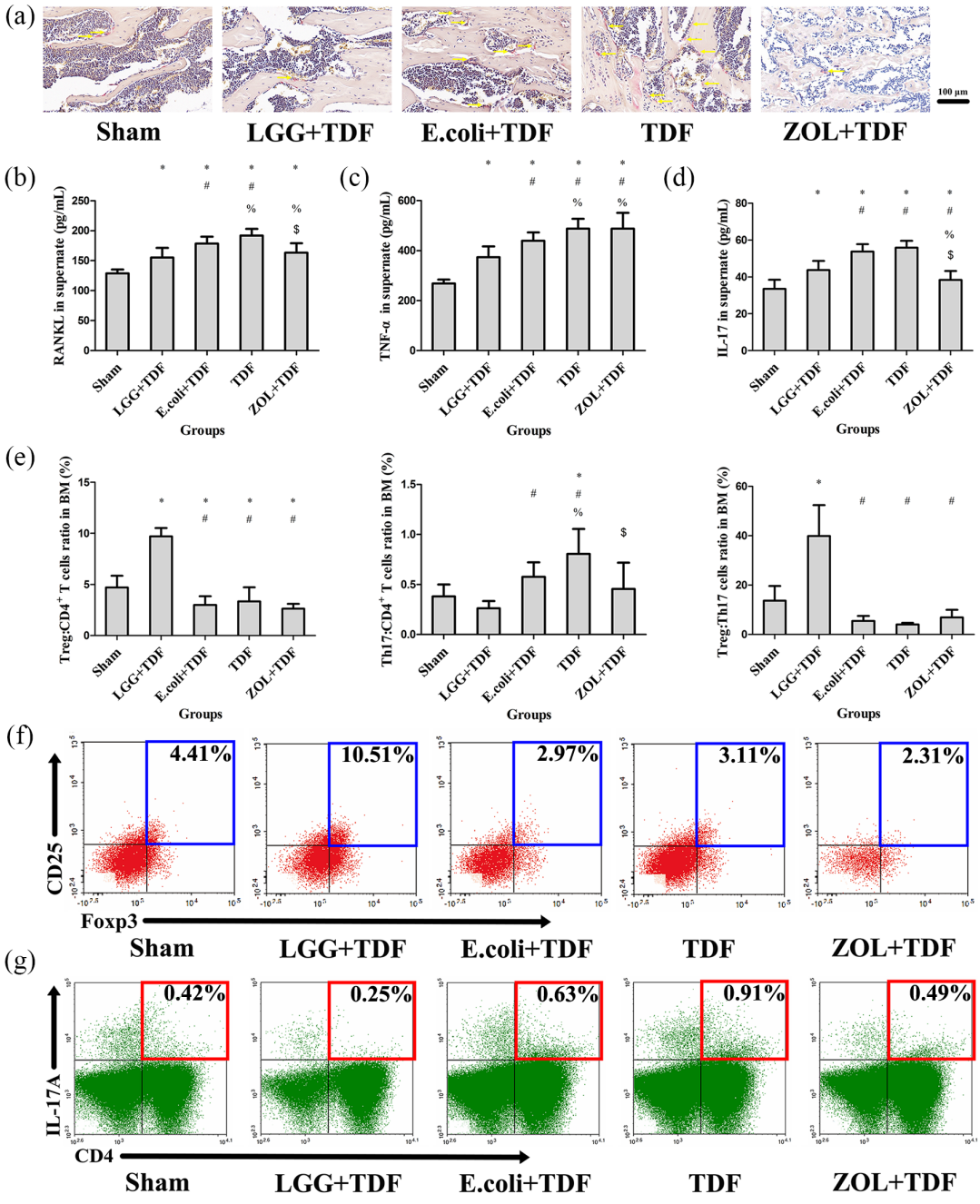

Figure 4. LGG administration protected against osteoclastogenesis and modulated the immune response in the BM.
(a) Representative images of bone marrow stained by TRAP in the femur (yellow arrows indicate claret-red osteoclast stained by TRAP). Scale bar = 100 μm. ELISA analysis of cell supernatant levels of RANKL (b), TNF-α (c), and IL-17 (d) ($n = 10$ mice per group). (e) FACS analysis on the ratios of Treg and Th17 cells in $CD4^+$ T cell subset and the Treg:Th17 cell ratio from the BM ($n = 6$ mice per group). (f) Representative FACS plots of the ratio of Treg cells in $CD4^+$ T cell subset of the BM. (g) Representative FACS plots of the ratio of Th17 cells in the $CD4^+$ T cell subset of the BM. Data are expressed as mean ± SD. All data were normally distributed according to the Shapiro–Wilk normality test and analyzed using two-way ANOVA and *post hoc* tests applying the LSD correction for multiple comparisons.
*$p < 0.05$ compared with the Sham group.
#$p < 0.05$ compared with the LGG+TDF group.
%$p < 0.05$ compared with the *E. coli*+TDF group.
$$p < 0.05$ compared with the TDF group.
ANOVA, analysis of variance; BM, bone marrow; ELISA, enzyme-linked immunosorbent assay; FACS, fluorescence-activated cell sorting; IL-17, interleukin-17; LGG, *Lactobacillus rhamnosus* GG; LSD, least significant difference; RANKL, receptor activator of nuclear factor kappa-B ligand; SD, standard deviation; TDF, tenofovir disoproxil fumarate; Th17, T-helper 17 cell; TNF-α, tumor necrosis factor alpha; TRAP, tartrate-resistant acid phosphatase; Treg, regulatory T cell; ZOL, zoledronic acid.

and Figure 4(a)]. Furthermore, the level of RANKL in the cell supernatant of BM-derived cells from LGG+TDF and ZOL+TDF groups also substantially decreased compared with that in the *E. coli*+TDF and TDF groups [$p < 0.05$, respectively; Figure 4(b)]; assessment of the transcript levels of *Rankl* and *Trap* showed similar results (Figure S4).

To explore whether osteoclastogenesis was related to inflammation, ELISA and FACS were performed. Compared with those in the *E. coli*+TDF and TDF groups, the concentrations of TNF-α and IL-17 in the cell supernatant were dramatically decreased in the LGG+TDF group ($p < 0.05$, respectively). Besides, the ZOL+TDF group had a significantly increased TNF-α level compared with that in the Sham, LGG+TDF, and *E. coli*+TDF groups, and a decreased IL-17 level compared with that in the LGG+TDF, *E. coli*+TDF, and TDF groups [$p < 0.05$, respectively; Figure 4(c,d)]. Moreover, the FACS results revealed that the ratio of Treg cells in the $CD4^+$ T cell subset and the Treg:Th17 cell ratio in the LGG+TDF group were the highest among the five groups ($p < 0.05$, respectively). In contrast, the proportion of Th17:$CD4^+$ T cells in the LGG+TDF group decreased dramatically compared with that in the *E. coli*+TDF and TDF groups ($p < 0.05$, respectively). Besides, the ZOL+TDF group had a significantly decreased proportion of Th17:$CD4^+$ T cells compared with that of the TDF group [$p < 0.05$; Figure 4(e–g)]. Consistent with these results, the data from qPCR showed that the messenger ribonucleic acid (mRNA) levels of *Tnfα*, *Il-17a*, *Il-1b*, and *Il-6* (osteoclastogenesis cytokines) in the LGG+TDF group were significantly decreased compared with those in the *E. coli*+TDF, TDF, and ZOL+TDF groups ($p < 0.05$, respectively). By contrast, the LGG+TDF group exhibited dramatically increased *Ifng* (an antiosteoclast cytokine) and *Foxp3* (forkhead box p3) mRNA levels compared with those in the *E. coli*+TDF, TDF, and Sham groups ($p < 0.05$, respectively). Notably, the ZOL+TDF group had the highest *Ifng* level among the five groups ($p < 0.05$, respectively; Figure S4).

LGG regulates intestinal inflammatory response and intestinal permeability

To explore the systemic inflammatory response induced by LGG, serum proinflammatory cytokines and lymphocytes of the spleen were detected. Consistent with the inflammatory response in the BM, serum RANKL, TNF-α, and IL-17 levels in the LGG+TDF group were lower than those in the *E. coli*+TDF and TDF groups ($p < 0.05$, respectively). Besides, the ZOL+TDF group had significantly decreased RANKL and IL-17 levels compared with those in the *E. coli*+TDF and TDF groups and increased TNF-α levels compared with those in the Sham and LGG+TDF groups [$p < 0.05$, respectively; Figure 5(a)]. Furthermore, compared with those in the *E. coli*+TDF and TDF groups, the LGG+TDF group had dramatically increased ratios of Treg:$CD4^+$ T cells and Treg:Th17 cells, and a decreased proportion of Th17:$CD4^+$ T cells ($p < 0.05$, respectively). The proportion of Th17:$CD4^+$ T cells in the ZOL+TDF group dramatically decreased compared with that in the *E. coli*+TDF and TDF groups [$p < 0.05$, respectively; Figure 5(b–d)].

To investigate whether the inflammatory response in the intestine triggers an initial systemic inflammatory response, histology, qPCR, and FACS assays were performed. The quantification of the area of inflammatory cell infiltration showed that the LGG+TDF, Sham, and ZOL+TDF groups had a significantly decreased area of inflammatory cell infiltration compared with that in the *E. coli*+TDF and TDF groups ($p < 0.05$, respectively) that were similar to the representative images on area of inflammatory cell infiltration in intestinal mucosa from intestinal slicing stained by H&E in the five groups [Figure S5(a)]. Further results for the lymphocytic ratio in MLNs revealed that the LGG+TDF group had dramatically increased ratios of Treg:$CD4^+$ T cells and Treg:Th17 cells, and a decreased proportion of Th17:$CD4^+$ T cells compared with those in the *E. coli*+TDF, TDF and Sham groups, which was similar to the data from the BM and spleen ($p < 0.05$, respectively). Notably, the changes in Treg and Th17 cells were more robust compared with those in the BM and spleen [Figure 6(a–c)]. Furthermore, the transcript levels of inflammation-related mRNAs also supported these results. Specifically, the mRNA levels of *Tnfα*, *Il17a*, *Il1b*, and *Il6* in the LGG+TDF group were lower than those in the *E. coli*+TDF and TDF groups ($p < 0.05$, respectively). However, there were significant increases in *Ifng* and *Foxp3* mRNA levels in the LGG+TDF group

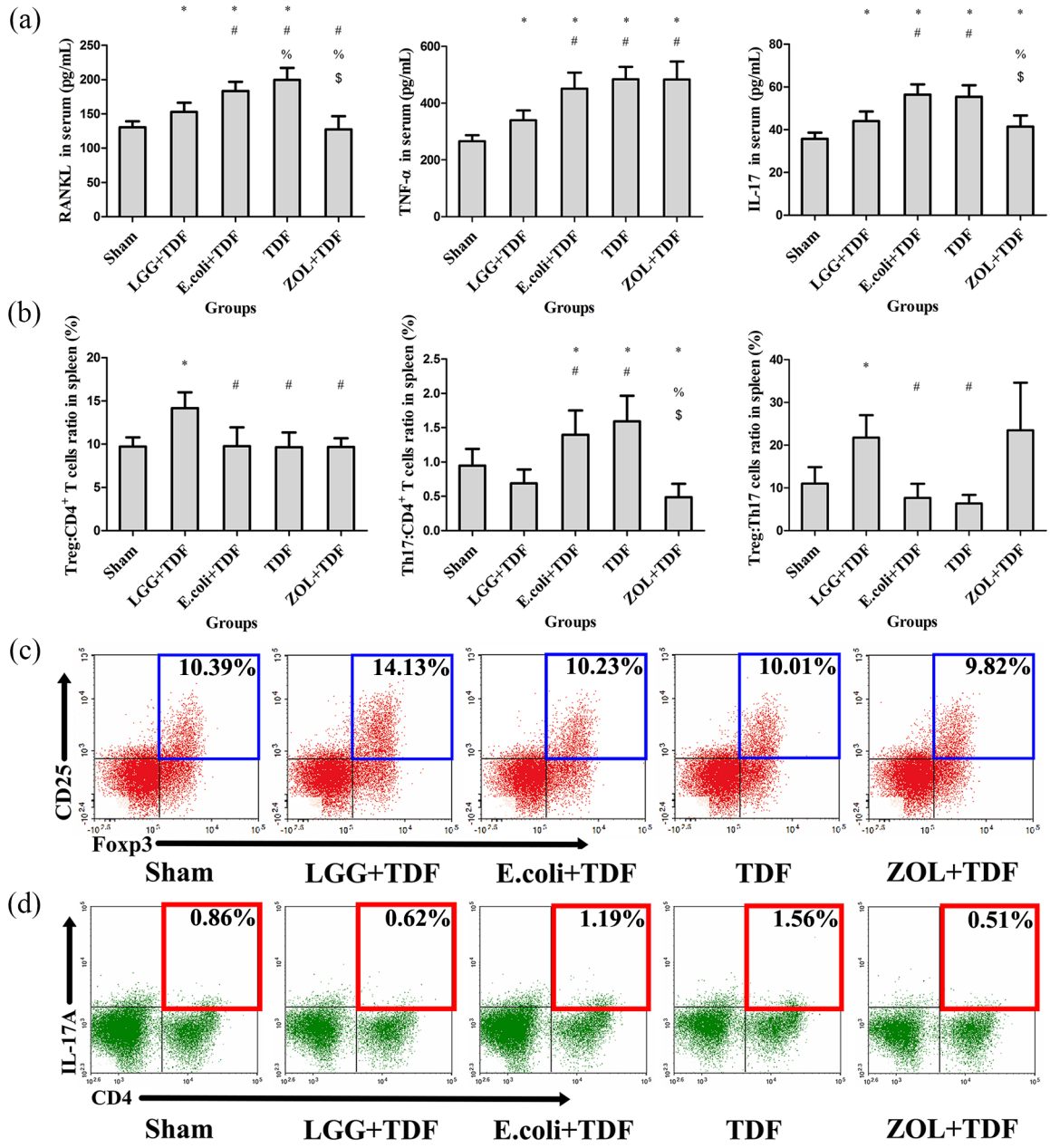

Figure 5. LGG regulated the systemic inflammatory response.
(a) ELISA analysis of serum levels of RANKL, TNF-α, and IL-17 ($n = 10$ mice per group). (b) FACS analysis of the ratios of Treg and Th17 cells in the $CD4^+$ T cell subset and the Treg:Th17 ratio in the spleen ($n = 6$ mice per group). (c) Representative FACS plots on ratio of Treg cells in the $CD4^+$ T cell subset of the spleen. (d) Representative FACS plots of the ratio of Th17 cells in the $CD4^+$ T cell subset of the spleen. Data are expressed as mean ± SD. All data were normally distributed according to the Shapiro–Wilk normality test and analyzed using two-way ANOVA and *post hoc* tests applying the LSD correction for multiple comparisons.
*$p < 0.05$ compared with the Sham group.
#$p < 0.05$ compared with the LGG+TDF group.
%$p < 0.05$ compared with the *E. coli*+TDF group.
$$p < 0.05$ compared with the TDF group.
ANOVA, analysis of variance; ELISA, enzyme-linked immunosorbent assay; FACS, fluorescence activate cell sorting; IL-17, interleukin-17; LGG, *Lactobacillus rhamnosus* GG; LSD, least significant difference; RANKL, receptor activator of nuclear factor kappa-B ligand; SD, standard deviation; TDF, tenofovir disoproxil fumarate; Th17, T-helper 17 cell; TNF-α, tumor necrosis factor alpha; TRAP, tartrate-resistant acid phosphatase; Treg, regulatory T cell; ZOL, zoledronic acid.

compared with those in the *E. coli*+TDF and TDF groups [$p < 0.05$, respectively; Figure S5(b)].

The inflammatory status of the gut is associated with changes in intestinal permeability.[33] The claudin family (CLDN) plays a key role in gap junction protein synthesis, which is important for physiological tightening of the intestinal barrier.[34] The results showed that the mRNA levels of *Cldn2*, *Cldn3*, and *Cldn15* were higher in the LGG+TDF and ZOL+TDF groups than in the *E. coli*+TDF and TDF groups, although the LGG+TDF group had dramatically increased *Cldn3* and *Cldn15* mRNA levels compared with those in the ZOL+TDF group [$p < 0.05$, respectively; Figure 6(d)]. Moreover, serum endotoxin (ET) and FD4 concentration levels increased dramatically in the LGG+TDF and ZOL+TDF groups compared with those in the *E. coli*+TDF, TDF, and Sham groups ($p < 0.05$, respectively), which showed indirectly that the LGG+TDF and ZOL+TDF groups had tighter intestinal barriers [Figure 6(e,f)].

LGG reconstructs the community structure and metabolite composition of the gut microbiota

To determine how LGG regulates the intestinal inflammatory response and intestinal permeability, the effects on the gut microbiota triggered by LGG were investigated. First, the overall diversity and structure of the intestinal microbial ecosystem was assessed. The data from 16S pyrosequencing of mice feces showed that 529 OTUs at 97% identity could be used to assess the differences among the groups. The shared and unique OTUs are illustrated in a Venn diagram [Figure 7(a)]. Moreover, the alpha diversity indices of Chao1, observed_species, and Shannon index in the LGG+TDF group were markedly decreased compared with those in the Sham, *E. coli*+TDF, or TDF groups ($p < 0.05$, respectively). Moreover, the ZOL+TDF group had the lowest Chao1 and observed_species index and highest goods_coverage index among the five groups ($p < 0.05$, respectively), which indicated that there were significant decreases in both bacterial diversity and richness in the guts of the LGG+TDF and ZOL+TDF groups (Table S4). In addition, PCoA based on the weighted UniFrac distances of OTU levels at 97% identity also revealed that the community structure of the LGG+TDF group was not analogous to that of the TDF group. However, the community structure of the ZOL+TDF group was totally different to those of the other four groups [Figure 7(b)]. Further analysis using LEFSe revealed significant differential microbiota compositions among the five groups. Notably, there were 21 preponderant microbiota in the ZOL+TDF group, which was the most among the five groups. In the LGG+TDF group, there were relatively higher abundances of *Lactococcus*, *Enterobacteriaceae*, *Clostridiaceae_1*, *Candidatus_Arthromitus*, and *Enterobacteriales*. However, the TDF group was enriched for *Ruminococcaceae_UCG_014* and *Marvinbryantia*, based on the LDA distribution histogram and cladogram. Moreover, the preponderant microbiota in the LGG+TDF, *E. coli*+TDF, TDF, and ZOL+TDF groups did not match with that of the Sham group [Figure 7(c) and Figure S6(a)]. A heatmap based on the taxonomy and species components analysis at the genus level showed the details of the different species and their abundance among the five groups [Figure S6(b,c)]. In addition, a co-occurrence network analysis based on the 52 most abundant genera revealed 56 positive associations and 18 negative associations in the network diagram. Notably, *Lactococcus* exhibited a high degree of positive linkage with *Candidatus_Arthromitus* among the highly abundant species in the LGG+TDF group [Figure S6(d)].

Secondly, metabolomics analysis of fecal samples was performed using UPLC-Q-TOF/MS to identify the differential metabolites between the LGG+TDF and TDF groups. A two-component OPLS-DA model indicated a definite separation between the LGG+TDF and TDF groups [Figure S7(a)]. Next, 116 differentially abundant metabolites, based on those having a VIP >1.0, were selected from 16,981 peaks using a two-component OPLS-DA model [Figure S7(b)]. Thereafter, considering the relative abundances of the metabolites between the two groups, 19 differentially abundant metabolites were chosen from 116 differentially abundant metabolites, based on a fold change (FC) >2.5 or FC <0.4 (ratio of LGG group relative to the TDF group; Table 2). In the table, eight kinds of glycerophospholipids were present among the 19 metabolites, which was the most of any metabolite group among the differentially abundant metabolites. However, six glycerophospholipids were present in the feces of the LGG+TDF group and two were present in the

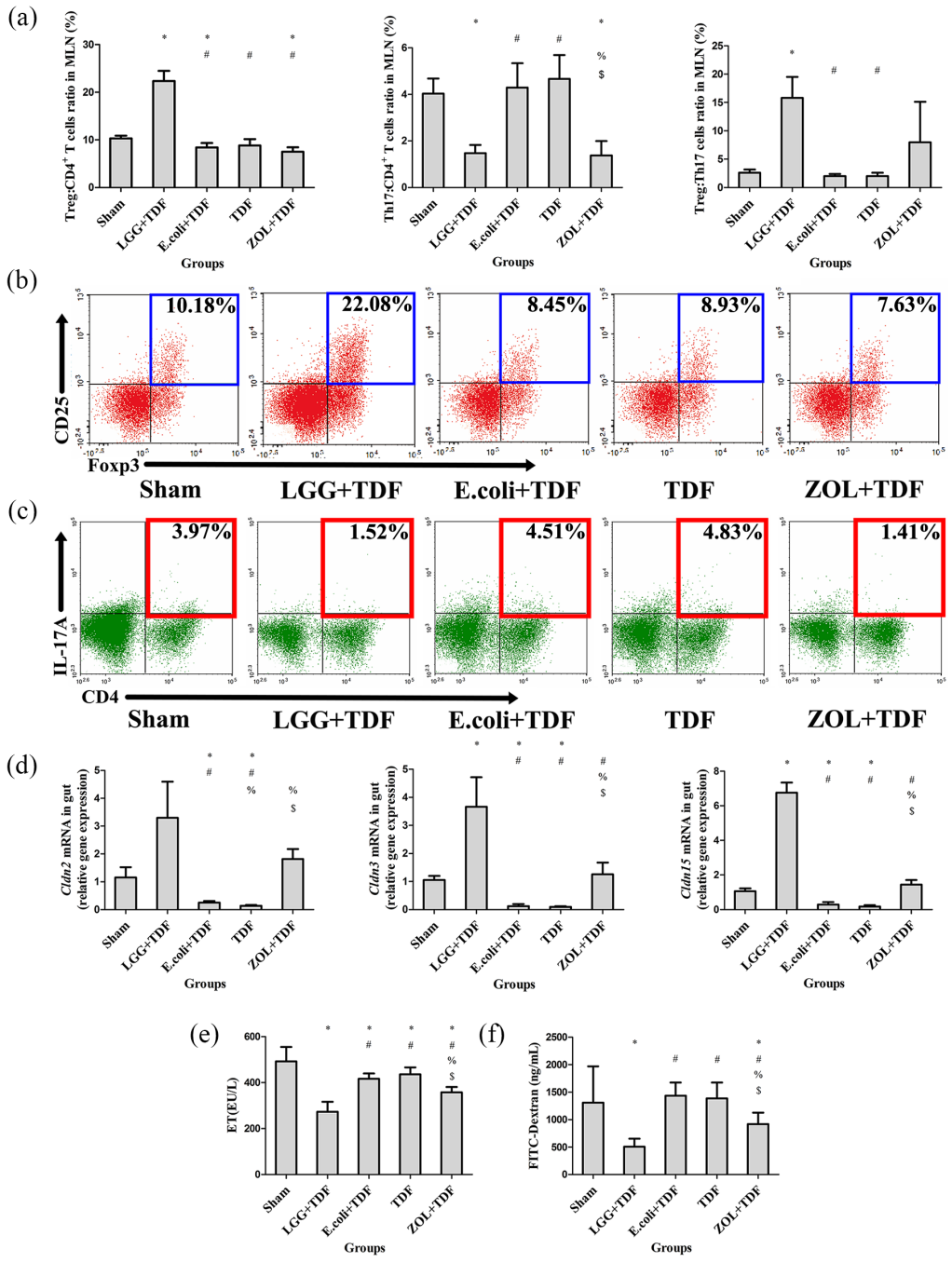

Figure 6. LGG regulated the intestinal inflammatory response and permeability.
(a) FACS analysis of Treg and Th17 cells in MLNs ($n = 6$ mice per group). (b) Representative FACS plots of ratio of Treg cells in the $CD4^+$ T cell subset of MLNs. (c) Representative FACS plots of the ratio of Th17 cells in the $CD4^+$ T cell subset of MLNs. (d) qPCR analysis measuring the transcript levels of the claudin family ($n = 6$ mice per group). (e) ELISA analysis of serum levels of ET ($n = 8$–10 mice per group). (f) Serum FD4 levels were measured in serum ($n = 9$–10 mice per group). Data are expressed as mean ± SD. All data were normally distributed according to the Shapiro–Wilk normality test and analyzed using two-way ANOVA and *post hoc* tests applying the LSD correction for multiple comparisons.
*$p < 0.05$ compared with the Sham group.
#$p < 0.05$ compared with the LGG+TDF group.
%$p < 0.05$ compared with the *E. coli*+TDF group.
$$p < 0.05$ compared with the TDF group.
ANOVA, analysis of variance; ELISA, enzyme-linked immunosorbent assay; ET, endotoxin; FD4, fluorescently labeled dextran; LGG, *Lactobacillus rhamnosus* GG; LSD, least significant difference; MLNs, mesenteric lymph nodes; qPCR, quantitative real-time polymerase chain reaction; TDF, tenofovir disoproxil fumarate; Th17, T-helper 17 cell; Treg, regulatory T cell; ZOL, zoledronic acid.

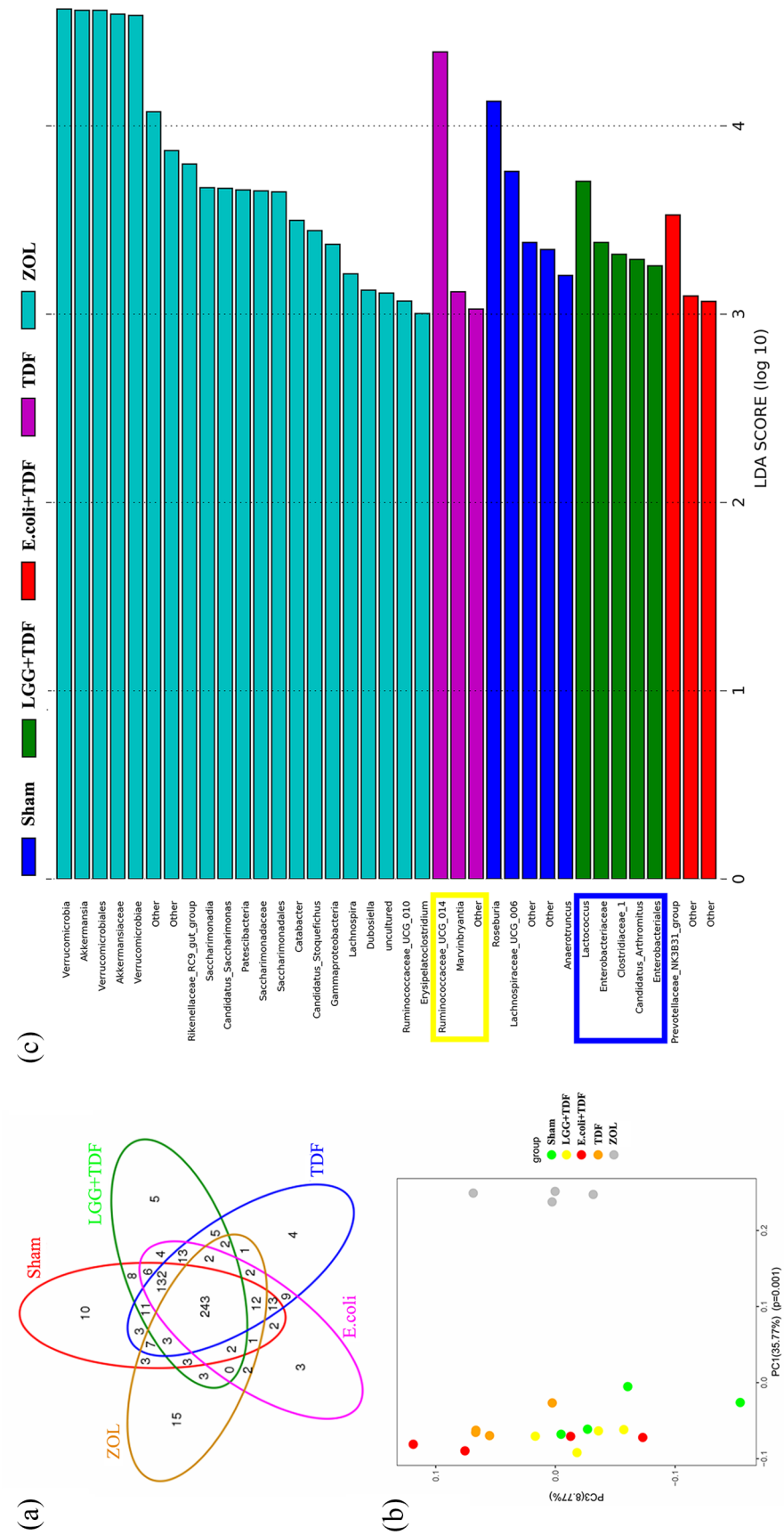

Figure 7. LGG reconstructed the intestinal microbial ecosystem at 8 weeks.
(a) A Venn diagram of shared and unique OTUs at 97% identity. (b) Beta diversity indices of the PCoA. PC1 and PC3 explained 35.77% and 8.77% of the variation observed, respectively ($p = 0.001$). (c) Histogram of the LDA scores showing significantly different microbiota compositions. The blue box represents highly abundant species in the LGG+TDF group. The yellow box represents highly abundant species in the TDF group.
LDA, linear discriminant analysis; LGG, *Lactobacillus rhamnosus* GG; OTUs, operational taxonomic units; PC1, principal component 1; PCoA, principal co-ordinates analysis; TDF, tenofovir disoproxil fumarate; ZOL, zoledronic acid.

Table 2. Differential metabolites identified from the OPLS-DA between the LGG+TDF and TDF groups (VIP > 1.0 and FC > 2.5 or < 0.4).

No.	Metabolites	Category	VIP	FC (LGG+TDF/TDF)	*p* value
1	LysoPC [20:3(5Z,8Z,11Z)]	Glycerophospholipid	1.661	6.768	0.020#
2	LysoPC [20:2(11Z,14Z)]	Glycerophospholipid	1.003	3.689	0.009#
3	L-alpha-Amino-1H-pyrrole-1-hexanoic acid	Organic acid	1.952	3.675	0.0002#
4	N-(heptan-4-yl)benzo[d][1,3]dioxole-5-carboxamide	Heterocyclic organic compounds	1.782	3.590	0.007#
5	PE-NMe (11:0/11:0)	Glycerophospholipid	1.458	3.374	0.008 #
6	PS (19:0/0:0)	Glycerophospholipid	1.208	3.314	0.004#
7	N-oleoyl tyrosine	Amino acid	4.343	3.152	0.014#
8	15-HETE-VA	Fatty amide	1.658	3.021	0.008#
9	9S-(2-cyclopentenyl)-1-nonanol	Aliphatic alcohol	2.201	3.021	0.001#
10	Lucidenic acid M	Triterpene	1.525	2.953	0.047#
11	LysoPC [22:1(13Z)]	Glycerophospholipid	4.607	2.680	0.001#
12	4,5-Dihydropiperlonguminine	Heterocyclic organic compounds	1.408	2.648	0.023#
13	Cer (d18:0/h17:0)	Sphingolipid	1.717	2.576	0.035#
14	LysoPC [20:1(11Z)]	Glycerophospholipid	1.001	2.549	0.006#
15	Reticulatamol	Aliphatic alcohol	1.659	0.384	0.003#
16	PE [20:1(11Z)/P-18:1(11Z)]	Glycerophospholipid	1.555	0.375	0.010#
17	PA [O-20:0/18:2(9Z,12Z)]	Glycerophospholipid	1.525	0.370	0.018#
18	Isoleucyl-phenylalanine	Amino acid	1.192	0.238	0.022#
19	N-acetyl-leukotriene E4	Eicosanoid	1.390	0.229	0.003#

#$p < 0.05$ compared with the LGG+TDF group.
FC, fold change; LGG, *Lactobacillus rhamnosus* GG; LysoPC, lysophosphatidylcholine; OPLS-DA, orthogonal partial least-squares-discriminant analysis; TDF, tenofovir disoproxil fumarate; VIP, variable importance in the projection.

feces of the TDF group. Accordingly, glycerophospholipid metabolism was increased in the LGG+TDF group compared with that in the TDF group ($p < 0.01$) based on analysis of the KEGG database [Figure S7(c)]. Moreover, there were four lysophosphatidylcholines (LysoPCs) in the six glycerophospholipids of the LGG+TDF group, which might have an anti-inflammatory ability by suppressing leukocyte infiltration, leukotrienes, and proinflammatory cytokines.[35–37] Notably, the metabolite N-acetyl-leukotriene E4 (N-acetyl LTE_4) had the highest relative abundance in the TDF group, which was markedly and positively linked with a number of pathophysiological characteristics, including inflammation, asthma, and thrombosis.[38]

Discussion

In this study, administration of LGG for 8 weeks reversed the loss of trabecular bone in the BM induced by TDF, which was consistent with the

results for other probiotics in previous studies.[39] Moreover, Ohlsson and colleagues stated that probiotics could protect against ovariectomization-induced cortical bone loss.[40] Our research also showed that LGG protected against the cortical bone loss induced by TDF, which is major determinant of bone strength. As expected, ZOL also exhibited excellent antiresorptive ability, especially in terms of Ma.BMD and BV/TV. Further biomechanical assays revealed that femurs treated with LGG had excellent biomechanical properties, especially the Young's modulus in the LGG+TDF group, which increased dramatically compared with that in the ZOL+TDF group, which has great significance in avoiding fragility fractures.[41] The biomechanical properties of the ZOL+TDF group were similar to those of the LGG+TDF group except for Young's modulus. Notably, we observed the BV/TV and Ma.BMD of the trabecular bone at different time points, and unlike in the ZOL+TDF group, there was a similar tendency to increase from baseline to 4 weeks and decrease from 4 weeks to 8 weeks in both the LGG+TDF and Sham groups, which indicated that the trabecular bone microarchitecture could not be maintained at a high level for a long time, although the bone microarchitecture at 8 weeks was analogous to the parameters at baseline. Surprisingly, the volume of cortical bone kept increasing and the %Ct.Ar was similar among the LGG+TDF, ZOL+TDF, and Sham groups at 8 weeks, which favored the bone mechanical properties.

Increasing evidence supports the hypothesis that the inflammatory response is closely associated with osteoclastogenesis.[42] Generally, osteoclastogenesis is regulated by the production of immune factors such as RANKL, TNF-α, and IL-17.[43] RANKL is secreted by many kinds of cells, such as hematopoietic cells, T cells, and B cells. As the primary factor of osteoclastogenesis, RANKL is highly expressed in subjects with HIV receiving TDF compared with subjects with HIV who did not receive TDF.[44] Several recent studies showed that TNF-α-mediated osteoclastogenesis was activated through potentiation of RANKL,[45] which was consistent with our results. Th17 cells, a type of $CD4^+$ T cell defined by its ability for IL-17 production, can also promote osteoclastogenesis by secreting IL-17, RANKL, TNF-α, IL-1, and IL-6.[46] Moreover, RANKL secretion from osteoblastic cells was increased by IL-17.[47] In the present study, higher expression of RANKL, TNF-α, and IL-17 was detected in both the BM supernatant and serum in the TDF group compared with that in the LGG+TDF group, which contributed to the osteoclastogenesis induced by TDF. However, as a subset of $CD4^+CD25^+$ T lymphocytes, Treg cells express the FOXP3 marker, which plays a key role in suppressing the inflammatory response.[48] For example, Xu and colleagues showed that triptolide could inhibit the bone resorption induced by osteoclastogenesis by enhancing the production of Treg cells *in vitro*.[49] Moreover, Tyagi and colleagues also showed that butyrate stimulates bone formation *via* a Treg-dependent mechanism.[50] Furthermore, McCabe and colleagues confirmed that *Lactobacillus reuteri* ATCC PTA 6475 could improve BMD by decreasing intestinal TNF-α levels.[51] Similar to these studies, we found that supplementation with LGG suppressed RANKL, TNF-α, and IL-17 production both in the BM supernatant and serum, decreased the proportion of Th17 cells, and boosted the Treg cell ratio in the BM, spleen, and MLN. Thus, we concluded that TDF-induced bone loss was suppressed by induction of Treg cells, at least partially. However, ZOL could not upregulate the Treg cell ratio in the BM, spleen, and MLNs, which means that ZOL suppresses the bone resorption triggered by TDF *via* pathways other than those involving Treg cells.

Administration of TDF facilitated the production of proinflammatory cytokines and the induction of Th17 cells. However, supplementation with LGG suppressed the inflammatory response by elevating Treg cell numbers. When TDF or LGG are administered by oral gavage, the intestinal barrier plays a key role in the relationship between TDF/LGG and the systemic immune response. The tight physiological barrier constructed by the intestinal epithelium, defined as the intestinal barrier, has an important function in separating the mammalian host from the gut microbiota. Generally, molecules of more than 15 Å cannot traffic between the gut lumen and the epithelial submucosa *via* the paracellular route under healthy physiological conditions.[52] By contrast, increased intestinal permeability leads to the translocation of a wider range of molecules, often resulting in intestinal and systemic proinflammatory responses.[33] Thus, it is essential for healthy subjects to maintain an intact physiological

intestinal barrier. Li and colleagues reported that probiotics prevented the increased intestinal permeability induced by sex steroid deficiency, which further resulted in attenuation of inflammation-related bone loss.[20] Furthermore, Chen and colleagues demonstrated that LGG supernatants ameliorated hepatic injury induced by chronic–binge alcohol by promoting the intestinal barrier function.[53] In this study, we also showed that LGG increased the intestinal barrier integrity and ameliorated bone loss. ZOL also exhibited an ability to increase intestinal barrier integrity, partially.

Given that TDF promotes increased intestinal permeability and LGG reversed it, how does TDF or LGG work in the gut? To answer this, we focused on the gut microbiota composition and related metabolites. The results showed that the bacterial diversity and richness of gut microbiota were reconstructed in both groups, suggesting that reconstruction of the gut microbiota triggered by LGG or TDF played a key role in regulating intestinal permeability and the inflammatory response. Furthermore, metabolomic analysis of fecal samples showed that that the most differentially abundant metabolites in the LGG+TDF group were LysoPCs, which exhibit excellent anti-inflammatory effects by inhibiting the formation of proinflammatory leukotrienes and cytokines such as TNF-α, IL-2, and IL-6.[35–37]

To the best of our knowledge, this research was the first to show that the preponderant metabolite N-acetyl LTE_4 from feces was detected after being administered to TDF by oral gavage. N-acetyl LTE_4 can be synthesized from leukotriene C4, leukotriene D4, and LTE_4[54] and triggers a number of pathophysiological effects, including inflammation, asthma, and thrombosis,[38] and is the probable source of the systematic inflammatory response triggered by TDF. Therefore, we concluded that the LysoPCs expressed by LGG-induced gut microbiota suppressed proinflammatory leukotrienes and the associated inflammatory response triggered by TDF, which may be a rational explanation for the initial role of LGG in the gut.

Generally, ZOL plays an antiosteoporotic role by suppressing the bone resorption induced by osteoclasts, directly.[55] In brief, ZOL has high affinity for hydroxyapatite and localizes preferentially at areas of high bone turnover, which can be released during bone resorption and is subsequently internalized by osteoclasts.[56] ZOL acts by inhibiting the mevalonate pathway in osteoclasts by suppressing farnesyl pyrophosphate synthase (FPPS) and preventing subsequent downstream protein prenylation.[57, 58] Finally, ZOL inhibits osteoclast formation and osteoclast-mediated bone resorption, and induces apoptosis of osteoclasts. However, bone formation induced by osteoblasts was almost unaffected at the early stage of ZOL ingestion. Hence, the bone mass and BMD of the femur will increase quickly after the administration of ZOL.

In this study, we found that the ZOL+TDF group had the lowest tibial MAR and BFR among the five groups, and less serum P1NP compared with that in the LGG+TDF group, which meant that bone formation was also suppressed after long-term ZOL ingestion. Previous studies similarly concluded that the MAR and BFR were inhibited after ZOL administration.[59,60] Besides, bone metabolism and osteointegration can be directly inhibited, and new bone formation further decreased, when ZOL is applied locally to grafted bones.[61,62] How does ZOL have an adverse function in bone formation? It may be associated with the gradual and mild suppressing the activity of osteoblasts by chronically administered ZOL. For example, ZOL inhibited the function of osteoblasts in a dose-dependent manner *in vitro*.[63–65] Moreover, ZOL also induced apoptosis of osteoblasts.[66]

We also showed that the TNF-α level in the BM was upregulated in the ZOL+TDF group compared with that in the LGG+TDF group. De Barros Silva and colleagues also showed that TNF-α from the periodontium of rats was increased by chronic treatment with ZOL.[67] Dhillon and colleagues suggested that γδ-T cells can be activated and expanded, subsequently releasing proinflammatory cytokines like TNF-α, IL-6, or interferon gamma, when FPPS was inhibited by ZOL.[68]

There are some limitations of this study. First, the in-depth mechanisms among TDF, N-acetyl LTE_4, and proinflammatory effects require further exploration. Second, the effect of LGG against TDF-induced osteoporosis should be further investigated based on an HIV/HBV infection

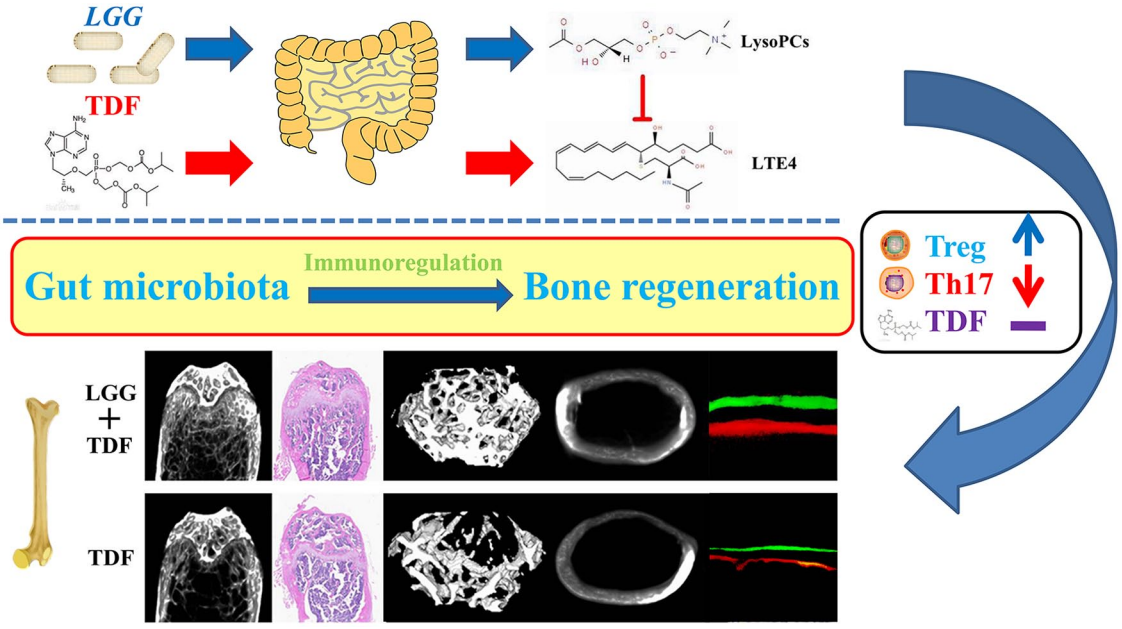

Figure 8. Schematic diagram of the effects and mechanisms of attenuating TDF-induced bone loss using LGG in mice.
LGG reconstructed the community structure of the gut microbiota and promoted the expression of preponderant metabolites (glycerophospholipids) to suppress TDF-induced N-acetyl LTE_4. LGG further improved the intestinal integrity and reversed the inflammatory response systemically, resulting in attenuation of TDF-induced bone loss in mice.
LGG, *Lactobacillus rhamnosus* GG; LTE_4, leukotriene E4; TDF, tenofovir disoproxil fumarate.

animal model, such as a Rhesus Macaque animal model infected with simian immunodeficiency virus.

In summary, LGG reconstructed the community structure of the gut microbiota and promoted the expression of preponderant metabolites (LysoPCs) to suppress TDF-induced leukotrienes. LGG further improved the intestinal integrity and inhibited the inflammatory response systemically, resulting in attenuation of TDF-induced bone loss in mice (Figure 8). Our study suggested a potential therapeutic strategy for using probiotics to prevent or treat TDF-induced osteoporosis.

Acknowledgements
We thank the Dental Material Research Center (Peking University School and Hospital of Stomatology) for assistance with the biomechanical and HPLC assays, and Shanghai Lu-Ming Biotech Co., Ltd. (Shanghai, China) for assistance with Metabonomics analysis.

Funding
The author(s) disclosed receipt of the following financial support for the research, authorship, and/or publication of this article: this work was supported by grants from the National Natural Science Foundation of China (grant number 81700935, 81870742, 81570953, and 81771039); the Project for Culturing Leading Talents in Scientific and Technological Innovation of Beijing (Z171100001117169); and a grant from the CAMS Innovation Fund for Medical Sciences (2017-I2M-1-014; http://www.pumc.edu.cn).

Conflict of interest statement
The authors declare that there is no conflict of interest.

ORCID iD
Yongsheng Zhou https://orcid.org/0000-0002-4332-0878

Supplemental material
Supplemental material for this article is available online.

References
1. Obiebi IP and Nwannadi EA. Tenofovir-induced renal tubular dysfunction among human immunodeficiency virus patients on antiretroviral

therapy in Nigeria: prospects for early detection of presymptomatic nephrotoxicity. *Kidney Res Clin Pract* 2018; 37: 230–238.

2. Moran CA, Weitzmann MN and Ofotokun I. The protease inhibitors and HIV-associated bone loss. *Curr Opin HIV AIDS* 2016; 11: 333–342.
3. Weitzmann MN and Ofotokun I. Physiological and pathophysiological bone turnover - role of the immune system. *Nat Rev Endocrinol* 2016; 12: 518–532.
4. Ofotokun I, Titanji K, Vunnava A, *et al*. Antiretroviral therapy induces a rapid increase in bone resorption that is positively associated with the magnitude of immune reconstitution in HIV infection. *AIDS* 2016; 30: 405–414.
5. Huang JS, Hughes MD, Riddler SA, *et al*. Bone mineral density effects of randomized regimen and nucleoside reverse transcriptase inhibitor selection from ACTG A5142. *HIV Clin Trials* 2013; 14: 224–234.
6. Wohl DA, Bhatti L, Small CB, *et al*. The ASSURE study: HIV-1 suppression is maintained with bone and renal biomarker improvement 48 weeks after ritonavir discontinuation and randomized switch to abacavir/lamivudine + atazanavir. *HIV Med* 2016; 17: 106–117.
7. Premaor MO and Compston JE. The hidden burden of fractures in people living with HIV. *JBMR Plus* 2018; 2: 247–256.
8. Post FA, Hamzah L and Fox J. Tenofovir disoproxil fumarate-associated bone loss: does vitamin D-binding protein play a role? *AIDS* 2017; 31: 178–179.
9. Paccou J, Viget N, Drumez E, *et al*. Prevalence and risk factors for low bone mineral density in antiretroviral therapy-naive HIV-infected young men. *Med Mal Infect* 2018; 48: 442–448.
10. Sharma A, Shi Q, Hoover DR, *et al*. Increased fracture incidence in middle-aged HIV-infected and HIV-uninfected women: updated results from the women's interagency HIV study. *J Acquir Immune Defic Syndr* 2015; 70: 54–61.
11. Skjodt MK, Frost M and Abrahamsen B. Side effects of drugs for osteoporosis and metastatic bone disease. *Br J Clin Pharmacol*. Epub ahead of print 17 October 2018. DOI: 10.1111/bcp.13759.
12. Barko PC, McMichael MA, Swanson KS, *et al*. The gastrointestinal microbiome: a review. *J Vet Intern Med* 2018; 32: 9–25.
13. Ohlsson C and Sjogren K. Effects of the gut microbiota on bone mass. *Trends Endocrinol Metab* 2015; 26: 69–74.
14. Alander M, Satokari R, Korpela R, *et al*. Persistence of colonization of human colonic mucosa by a probiotic strain, Lactobacillus rhamnosus GG, after oral consumption. *Appl Environ Microbiol* 1999; 65: 351–354.
15. Wang Y, Kirpich I, Liu Y, *et al*. Lactobacillus rhamnosus GG treatment potentiates intestinal hypoxia-inducible factor, promotes intestinal integrity and ameliorates alcohol-induced liver injury. *Am J Pathol* 2011; 179: 2866–2875.
16. Khailova L, Baird CH, Rush AA, *et al*. Lactobacillus rhamnosus GG improves outcome in experimental pseudomonas aeruginosa pneumonia: potential role of regulatory T cells. *Shock* 2013; 40: 496–503.
17. Salminen MK, Tynkkynen S, Rautelin H, *et al*. The efficacy and safety of probiotic Lactobacillus rhamnosus GG on prolonged, noninfectious diarrhea in HIV patients on antiretroviral therapy: a randomized, placebo-controlled, crossover study. *HIV Clin Trials* 2004; 5: 183–191.
18. Zhang Y. *Pharmacology experiment*. 2nd ed. Beijing, China: People's Medical Publishing House, 1996; 354.
19. Liu YS, Ou ME, Liu H, *et al*. The effect of simvastatin on chemotactic capability of SDF-1alpha and the promotion of bone regeneration. *Biomaterials* 2014; 35: 4489–4498.
20. Li JY, Chassaing B, Tyagi AM, *et al*. Sex steroid deficiency-associated bone loss is microbiota dependent and prevented by probiotics. *J Clin Invest* 2016; 126: 2049–2063.
21. Liu H, Li W, Liu Y, *et al*. Co-administration of aspirin and allogeneic adipose-derived stromal cells attenuates bone loss in ovariectomized rats through the anti-inflammatory and chemotactic abilities of aspirin. *Stem Cell Res Ther* 2015; 6: 200.
22. Kimble RB, Bain S and Pacifici R. The functional block of TNF but not of IL-6 prevents bone loss in ovariectomized mice. *J Bone Miner Res* 1997; 12: 935–941.
23. Liu H, Gao K, Lin H, *et al*. Relative skeletal effects in different sites of the mandible with the proximal tibia during ovariectomy and the subsequent estrogen treatment. *J Oral Implantol* 2015; 41: 386–390.
24. Yan J, Herzog JW, Tsang K, *et al*. Gut microbiota induce IGF-1 and promote bone formation and

growth. *Proc Natl Acad Sci U S A* 2016; 113: E7554–E7563.

25. Bouxsein ML, Boyd SK, Christiansen BA, *et al.* Guidelines for assessment of bone microstructure in rodents using micro-computed tomography. *J Bone Miner Res* 2010; 25: 1468–1486.

26. Liu H, Li W, Liu C, *et al.* Incorporating simvastatin/poloxamer 407 hydrogel into 3D-printed porous Ti6Al4V scaffolds for the promotion of angiogenesis, osseointegration and bone ingrowth. *Biofabrication* 2016; 8: 045012.

27. Liu H, Li W, Ge X, *et al.* Coadministration of puerarin (low dose) and zinc attenuates bone loss and suppresses bone marrow adiposity in ovariectomized rats. *Life Sci* 2016; 166: 20–26.

28. Prasad TR, Joseph S, Kole P, *et al.* Enantioselective supercritical fluid chromatography-tandem mass spectrometry method for simultaneous estimation of risperidone and its 9-hydroxyl metabolites in rat plasma. *Bioanalysis* 2017; 9: 1739–1750.

29. Luz-Crawford P, Kurte M, Bravo-Alegria J, *et al.* Mesenchymal stem cells generate a CD4+CD25+Foxp3+ regulatory T cell population during the differentiation process of Th1 and Th17 cells. *Stem Cell Res Ther* 2013; 4: 65.

30. Fan C, Jia L, Zheng Y, *et al.* MiR-34a promotes osteogenic differentiation of human adipose-derived stem cells via the RBP2/NOTCH1/CYCLIN D1 coregulatory network. *Stem Cell Reports* 2016; 7: 236–248.

31. Xiao C, Ran S, Huang Z, *et al.* Bacterial diversity and community structure of supragingival plaques in adults with dental health or caries revealed by 16S pyrosequencing. *Front Microbiol* 2016; 7: 1145.

32. Li H, Cai J, Chen R, *et al.* Particulate matter exposure and stress hormone levels: a randomized, double-blind, crossover trial of air purification. *Circulation* 2017; 136: 618–627.

33. Michielan A and D'Inca R. Intestinal permeability in inflammatory bowel disease: pathogenesis, clinical evaluation, and therapy of leaky gut. *Mediators Inflamm* 2015; 2015: 628157.

34. Zeissig S, Burgel N, Gunzel D, *et al.* Changes in expression and distribution of claudin 2, 5 and 8 lead to discontinuous tight junctions and barrier dysfunction in active Crohn's disease. *Gut* 2007; 56: 61–72.

35. Hung ND, Kim MR and Sok DE. Mechanisms for anti-inflammatory effects of 1-[15(S)-hydroxyeicosapentaenoyl] lysophosphatidylcholine, administered intraperitoneally, in zymosan A-induced peritonitis. *Br J Pharmacol* 2011; 162: 1119–1135.

36. Hung ND, Kim MR and Sok DE. Oral administration of 2-docosahexaenoyl lysophosphatidylcholine displayed anti-inflammatory effects on zymosan A-induced peritonitis. *Inflammation* 2011; 34: 147–160.

37. Zhong W, Li Q, Xie G, *et al.* Dietary fat sources differentially modulate intestinal barrier and hepatic inflammation in alcohol-induced liver injury in rats. *Am J Physiol Gastrointest Liver Physiol* 2013; 305: G919–932.

38. Celardo A, Dell'Elba G, Manarini S, *et al.* Kinetics of endogenous leukotriene B4 and E4 production following injection of the chemotactic peptide FMLP in the rabbit. *Prostaglandins* 1997; 54: 699–711.

39. Sjogren K, Engdahl C, Henning P, *et al.* The gut microbiota regulates bone mass in mice. *J Bone Miner Res* 2012; 27: 1357–1367.

40. Ohlsson C, Engdahl C, Fak F, *et al.* Probiotics protect mice from ovariectomy-induced cortical bone loss. *PLoS One* 2014; 9: e92368.

41. Wen XX, Wang FQ, Xu C, *et al.* Time related changes of mineral and collagen and their roles in cortical bone mechanics of ovariectomized rabbits. *PLoS One* 2015; 10: e0127973.

42. Kroner J, Kovtun A, Kemmler J, *et al.* Mast cells are critical regulators of bone fracture-induced inflammation and osteoclast formation and activity. *J Bone Miner Res* 2017; 32: 2431–2444.

43. Akbar MA, Nardo D, Chen MJ, *et al.* Alpha-1 antitrypsin inhibits RANKL-induced osteoclast formation and functions. *Mol Med* 2017; 23: 57–69.

44. Brown TT, Moser C, Currier JS, *et al.* Changes in bone mineral density after initiation of antiretroviral treatment with tenofovir disoproxil fumarate/emtricitabine plus atazanavir/ritonavir, darunavir/ritonavir, or raltegravir. *J Infect Dis* 2015; 212: 1241–1249.

45. Kanzaki H, Makihira S, Suzuki M, *et al.* Soluble RANKL cleaved from activated lymphocytes by TNF-alpha-converting enzyme contributes to osteoclastogenesis in periodontitis. *J Immunol* 2016; 197: 3871–3883.

46. Kikuta J, Wada Y, Kowada T, *et al.* Dynamic visualization of RANKL and Th17-mediated osteoclast function. *J Clin Invest* 2013; 123: 866–873.

47. Li JY, D'Amelio P, Robinson J, *et al.* IL-17A is increased in humans with primary hyperparathyroidism and mediates PTH-induced bone loss in mice. *Cell Metab* 2015; 22: 799–810.
48. Furukawa A, Wisel SA and Tang Q. Impact of immune-modulatory drugs on regulatory T cell. *Transplantation* 2016; 100: 2288–2300.
49. Xu H, Zhao H, Lu C, *et al*. Triptolide inhibits osteoclast differentiation and bone resorption in vitro via enhancing the production of IL-10 and TGF-beta1 by regulatory T cells. *Mediators Inflamm* 2016; 2016: 8048170.
50. Tyagi AM, Yu M, Darby TM, *et al*. The microbial metabolite butyrate stimulates bone formation via T regulatory cell-mediated regulation of WNT10B expression. *Immunity* 2018; 49: 1116–1131 e1117.
51. McCabe LR, Irwin R, Schaefer L, *et al*. Probiotic use decreases intestinal inflammation and increases bone density in healthy male but not female mice. *J Cell Physiol* 2013; 228: 1793–1798.
52. Fasano A. Leaky gut and autoimmune diseases. *Clin Rev Allergy Immunol* 2012; 42: 71–78.
53. Chen RC, Xu LM, Du SJ, *et al*. Lactobacillus rhamnosus GG supernatant promotes intestinal barrier function, balances Treg and TH17 cells and ameliorates hepatic injury in a mouse model of chronic-binge alcohol feeding. *Toxicol Lett* 2016; 241: 103–110.
54. Samhoun MN, Conroy DM and Piper PJ. Pharmacological profile of leukotrienes E4, N-acetyl E4 and of four of their novel omega- and beta-oxidative metabolites in airways of guinea-pig and man in vitro. *Br J Pharmacol* 1989; 98: 1406–1412.
55. Nancollas GH, Tang R, Phipps RJ, *et al*. Novel insights into actions of bisphosphonates on bone: differences in interactions with hydroxyapatite. *Bone* 2006; 38: 617–627.
56. Russell RG. Bisphosphonates: from bench to bedside. *Ann N Y Acad Sci* 2006; 1068: 367–401.
57. Coxon FP, Helfrich MH, Van't Hof R, *et al.* Protein geranylgeranylation is required for osteoclast formation, function, and survival: inhibition by bisphosphonates and GGTI-298. *J Bone Miner Res* 2000; 15: 1467–1476.
58. Dunford JE, Thompson K, Coxon FP, *et al*. Structure-activity relationships for inhibition of farnesyl diphosphate synthase in vitro and inhibition of bone resorption in vivo by nitrogen-containing bisphosphonates. *J Pharmacol Exp Ther* 2001; 296: 235–242.
59. Moe SM, Chen NX, Newman CL, *et al*. A comparison of calcium to zoledronic acid for improvement of cortical bone in an animal model of CKD. *J Bone Miner Res* 2014; 29: 902–910.
60. Allen MR, Chen NX, Gattone VH 2nd, *et al*. Skeletal effects of zoledronic acid in an animal model of chronic kidney disease. *Osteoporos Int* 2013; 24: 1471–1481.
61. Olejnik C, Falgayrac G, During A, *et al*. Doses effects of zoledronic acid on mineral apatite and collagen quality of newly-formed bone in the rat's calvaria defect. *Bone* 2016; 89: 32–39.
62. Belfrage O, Isaksson H and Tagil M. Local treatment of a bone graft by soaking in zoledronic acid inhibits bone resorption and bone formation. A bone chamber study in rats. *BMC Musculoskelet Disord* 2012; 13: 240.
63. Basso FG, SilveiraTurrioni AP, Hebling J, *et al*. Zoledronic acid inhibits human osteoblast activities. *Gerontology* 2013; 59: 534–541.
64. Yang X, Lu Y, Li Z, *et al*. Low concentrations of zoledronic acid are better at regulating bone formation and repair. *Intractable Rare Dis Res* 2013; 2: 18–23.
65. Orriss IR, Key ML, Colston KW, *et al.* Inhibition of osteoblast function in vitro by aminobisphosphonates. *J Cell Biochem* 2009; 106: 109–118.
66. Patntirapong S, Singhatanadgit W, Chanruangvanit C, *et al*. Zoledronic acid suppresses mineralization through direct cytotoxicity and osteoblast differentiation inhibition. *J Oral Pathol Med* 2012; 41: 713–720.
67. De Barros Silva PG, Ferreira Junior AEC, De Oliveira CC, *et al.* Chronic treatment with zoledronic acid increases inflammatory markers in periodontium of rats. *J Oral Pathol Med* 2017; 46: 1046–1053.
68. Dhillon S. Zoledronic acid (Reclast®, Aclasta®): a review in osteoporosis. *Drugs* 2016; 76: 1683–1697.